The Astrophysical Journal, 670:565–583, 2007 November 20

A COMPREHENSIVE ANALYSIS OF *SWIFT* XRT DATA. II. DIVERSE PHYSICAL ORIGINS OF THE SHALLOW DECAY SEGMENT

En-Wei Liang,[1,2] Bin-Bin Zhang,[1,3] and Bing Zhang[1]

Received 2007 April 30; accepted 2007 July 24

ABSTRACT

The origin of the shallow decay segment in *Swift* XRT light curves remains a puzzle. We analyze the properties of this segment with a sample of 53 long *Swift* GRBs detected before 2007 February. We show that the distributions of the sample's characteristics are lognormal or normal, and its isotropic X-ray energy ($E_{\rm iso,X}$) is linearly correlated with the prompt gamma-ray energy but with a steeper photon spectrum, aside from some X-ray flashes. No significant spectral evolution is observed from this phase to the following phase, and the latter is usually consistent with external-shock models, implying that the shallow decay is also of external-shock origin, likely a refreshed external shock. Within the refreshed-shock model, the data are generally consistent with a roughly constant injection luminosity up to the end of this phase, t_b. A positive correlation between $E_{\rm iso,X}$ and t_b also favors this scenario. Among the 13 bursts that have well-sampled optical light curves, six have an optical break around t_b and the breaks are consistent with being achromatic. However, the other seven either do not show an optical break or have a break at an epoch different from t_b. This raises a concern for the energy injection scenario, suggesting that the optical and X-ray emission may not be the same component, at least for some bursts. There are four significant outliers in the sample, GRBs 060413, 060522, 060607A, and 070110. The shallow decay phase in these bursts is immediately followed by a very steep decay after t_b, which is inconsistent with any external-shock model. The optical data for these bursts evolve independently from the X-ray data. These X-ray plateaus likely have an internal origin and demand continuous operation of a long-term central engine. We conclude that the observed shallow decay phase likely has diverse physical origins.

Subject headings: gamma rays: bursts — radiation mechanisms: nonthermal — X-rays: general

Online material: color figures

1. INTRODUCTION

Observations of the gamma-ray burst (GRB) phenomenon with the *Swift* satellite (Gehrels et al. 2004) have revolutionized our understanding of GRBs in many aspects (see recent reviews by Mészáros 2006; Zhang 2007). In its first 2 years of operation, the onboard X-Ray Telescope (XRT; Burrows et al. 2004) has accumulated a large set of well-sampled X-ray light curves from tens of seconds to days (even months) past the GRB triggers.

The generally accepted GRB models are the relativistic fireball models (Rees & Mészáros 1994; Mészáros & Rees 1997a; Sari et al. 1998; see reviews by Mészáros 2002; Zhang & Mészáros 2004; Piran 2005). These invoke a fireball powered by a GRB central engine that ejects an intermittent, relativistic outflow. Internal shocks from stochastic collisions within the ejecta power the observed prompt gamma rays, and deceleration of the fireball by the ambient medium excites a long-term external forward shock that powers the broadband afterglow (Mészáros & Rees 1997a; Sari et al. 1998). *Swift* data suggest possible late internal shocks as the origin of the erratic late X-ray flares seen in XRT light curves (Burrows et al. 2005; Fan & Wei 2005; King et al. 2005; Zhang et al. 2006; Dai et al. 2006; Proga & Zhang 2006; Perna et al. 2006). The XRT light curves generally begin with a rapidly decaying segment (Tagliaferri et al. 2005; O'Brien et al. 2006b), which is explained as the prompt emission tail due to the so-called curvature effect (Kumar & Panaitescu 2000b; Zhang et al. 2006; Liang et al. 2006; Yamazaki et al. 2006).[4] The broadband afterglows, which usually decay as a power law with index $\alpha \sim -1$ (the normal decay phase), are believed to be related to the external shock. If the external shocks are refreshed by continuous energy injection into the blast wave, a shallow decay phase prior to the normal decay phase could be observed (Rees & Mészáros 1998; Dai & Lu 1998a, 1998b; Panaitescu et al. 1998; Sari & Mészáros 2000; Zhang & Mészáros 2001; Wang & Dai 2001; Dai 2004; Granot & Kumar 2006; Panaitescu 2007; Yu & Dai 2007; see Zhang 2007 for a review).

As the fireball is decelerated by the ambient medium, the normal decay phase undergoes a transition to a jetlike decay phase (with decay index $\alpha \sim -2$) when the bulk Lorentz factor is degraded to $\Gamma \sim \theta_j^{-1}$, where θ_j is the opening angle of a conical jet (Rhoads 1997; Sari et al. 1999). Therefore, four successive emission episodes are invoked in the framework of the fireball models—a prompt gamma-ray phase with a tail, a shallow decay phase, a normal decay phase, and a jetlike decay phase. These power-law segments, together with erratic X-ray flares, compose a canonical X-ray afterglow light curve as revealed by *Swift* (Zhang et al. 2006; Nousek et al. 2006; O'Brien et al. 2006b). The physical origins of these segments have been discussed in the literature (Zhang et al. 2006; Nousek et al. 2006; Panaitescu et al. 2006b). Empirically, O'Brien et al. (2006a, 2006b) and Willingale et al. (2007) show that the data can be fitted by the superposition of a prompt emission component and an afterglow component.

In order to explore the physical origin of this canonical afterglow light curve, we are performing a systematic analysis of the *Swift* XRT data. In the first paper of this series (Zhang et al. 2007c,

[1] Department of Physics and Astronomy, University of Nevada, Las Vegas, Las Vegas, NV 89154; lew@physics.unlv.edu; zbb@physics.unlv.edu; bzhang@physics.unlv.edu.

[2] Department of Physics, Guangxi University, Nanning, 530004 Guangxi, China.

[3] National Astronomical Observatories/Yunnan Observatory, Chinese Academy of Sciences, Kunming, 650011 Yunnan, China.

[4] Other suggestions for interpreting this segment include cooling of a hot cocoon surrounding the GRB jet (Pe'er et al. 2006) and a highly radiative blast wave (Dermer 2007).

hereafter Paper I), we studied the steep decay phase for a sample of bright tails and revealed an apparent hard-to-soft spectral evolution for some bursts (see also Campana et al. 2006; Mangano et al. 2007; Butler & Kocevski 2007). This paper focuses on the shallow decay phase and the subsequent phase. This is motivated by some puzzling facts related to the shallow decay phase. For example, simultaneous X-ray and optical observations suggest that the break between the shallow and the normal decay segments in the X-ray band for some GRBs is chromatic (Panaitescu et al. 2006a; Fan & Piran 2006). This is inconsistent with the simplest energy injection model. One fundamental question is whether X-ray and optical afterglows have the same physical origin. Another interesting fact is that the XRT light curve of GRB 070110 shows a long-lived plateau followed by an abrupt falloff (the decay slope is about -9, with time zero at the trigger). This feature is hard to interpret within the external-shock models, and it likely indicates a long-lasting central-engine emission component (Troja et al. 2007).

Theoretically, several models have been proposed to interpret the shallow decay phase (see, e.g., Zhang 2007 for a review). Besides the energy injection models (Zhang et al. 2006; Nousek et al. 2006; Panaitescu et al. 2006b), the others include a combination of the GRB tail with delayed onset of the afterglow emission (Kobayashi & Zhang 2007), off-beam jets (Toma et al. 2006; Eichler & Granot 2006), precursor activity (Ioka et al. 2006), two-component jets (Granot et al. 2006; Jin et al. 2007), and varying microphysical parameters (Ioka et al. 2006; Panaitescu et al. 2006a; Fan & Piran 2006; Granot et al. 2006). The chromatism of some X-ray shallow-to-normal breaks has driven several ideas that go beyond the traditional external forward shock model. For example, Shao & Dai (2007) interpret the X-ray light curve as being due to dust scattering of some prompt X-rays, so that it has nothing to do with the external shock. Uhm & Beloborodov (2007) and Genet et al. (2007) interpret both X-ray and optical afterglows as emission from a long-lived reverse shock. Ghisellini et al. (2007) even suggested that the shallow-to-normal transition in X-ray afterglows may be produced by late internal shocks and that the end of this phase is due to the effect of beaming in the prompt ejecta (see also Nava et al. 2007).

The observational puzzles and theoretical chaos call for a systematic understanding of the shallow decay phase data for a large sample of GRBs. In particular, it is desirable to find out how bad the standard external forward shock model is when confronted with the data, for example, what fraction of bursts actually call for models beyond the standard external forward shock model. This is the primary goal of this paper. Data reduction and sample selection are presented in § 2. The characteristics of the shallow decay segment and their relations with the prompt gamma-ray phase are explored in § 3. In § 4, we test the external origin of the power-law segment following the shallow decay phase and explore whether or not the shallow decay segment is also of external origin. Assuming an energy injection model for the shallow decay phase, we further analyze the energy injection model parameters of these bursts in § 5. The relation among the isotropic X-ray energy ($E_{\rm iso,X}$), the peak energy of the prompt gamma-ray νf_ν spectrum (E_p), and t_b is investigated in § 6. The results are summarized in § 7 with some discussion. Throughout, the cosmological parameters $H_0 = 71$ km s^{-1} Mpc^{-1}, $\Omega_M = 0.3$, and $\Omega_\Lambda = 0.7$ have been adopted.

2. DATA REDUCTION AND SAMPLE SELECTION

The XRT data were taken from the *Swift* data archive. We developed a script to automatically download and maintain all the XRT data. The HEAsoft packages, including XSPEC, XSELECT, XIMAGE, and *Swift* data analysis tools, are used for the data reduction. We have developed an IDL code to automatically process the XRT data for a given burst in any user-specified time interval. Our procedure is described in what follows. The details of our code have been presented in Paper I.

Our code first runs the XRT tool `xrtpipeline` to reproduce the XRT clean event data and then makes pile-up corrections with the same methods as discussed by Romano et al. (2006; for the Window Timing [WT] mode data) and Vaughan et al. (2006; for the Photon Counting [PC] mode data). Both the source and background regions are annuli (for PC) or rectangular annuli (for WT). The inner radii of the annuli are dynamically determined by fitting the source brightness profiles with a King (1971) point-spread function (for PC) or determined from the photon flux using the method described by Romano et al. (2006; for WT). If the pile-up effect is not significant, the source regions are in the shape of a circle with radius $R = 20$ pixels (for PC) or a 40×20 pixel rectangle (for WT) centered at the burst position. The background regions have the same size as the source region, but at a distance of 20 pixels from the source region. Exposure correction is also performed, with an exposure map created by the XRT tool `xrtexpomap`. By considering these corrections, the code extracts the background-subtracted light curve and spectrum for the whole XRT data set. The signal-to-noise ratio is normally taken as 3 σ, but it is not rigidly fixed at this value and may be flexibly adjusted depending on the source brightness.

With our code we processed all the XRT data observed between 2005 February and 2007 January. We inspected all the light curves to identify the beginning (t_1) of the shallow decay segment and the end (t_2) of the decay phase following the shallow phase (which usually is the normal decay phase, but in some cases the decay slope could be much steeper). Note that the selection of t_1 and t_2 is guided by eye without a rigid criterion. Generally, t_1 is taken as the end of the steep decay segment or the beginning of the observation time, unless significant flares or high-level emission bumps following the GRB tails were observed. The ending time t_2 is taken as the end of the observation time except for GRBs 050416A, 050803, 060413, 060908, 060522, 061121, and 070110, which have an additional break at later times, in which case t_2 is chosen as that break time. For example, GRBs 060522 and 070110 have a distinct "normal decay" emission component following the sharp decay segment, and t_2 is taken as the end of the sharp decay. The last data points for GRBs 050416A, 050803, 060413, 060908, and 061121 show a flattening feature, which significantly deviates from the power-law decay trend post-t_b. We thus do not include those data points.

Physically, a temporal break of external-shock origin should be smooth (because of the equal arrival time effect in a relativistic shell of conical geometry). Therefore, a smoothed broken power law is used to fit the light curve in the time interval $[t_1, t_2]$:

$$F = F_0 \left[\left(\frac{t}{t_b} \right)^{\omega\alpha_1} + \left(\frac{t}{t_b} \right)^{\omega\alpha_2} \right]^{-1/\omega}, \quad (1)$$

where ω describes the sharpness of the break—the larger the ω, the sharper the break. In order to constrain ω, it is required that the time interval cover a range from $t_1 \ll t_b$ to $t_2 \gg t_b$ and that the light curve around t_b be well sampled. The parameter t_b is not significantly affected by ω, but both α_1 and α_2 are. We compare the results of fitting with $\omega = 1$ and $\omega = 3$ for the bursts in our sample (see below) in Figure 1. We find that, systematically, $t_b^{\omega=1} \sim t_b^{\omega=3}$, $\alpha_1^{\omega=1} < \alpha_1^{\omega=3}$, and $\alpha_2^{\omega=1} > \alpha_2^{\omega=3}$. We note that Willingale et al. (2007) fitted the XRT light curves with a superposition model

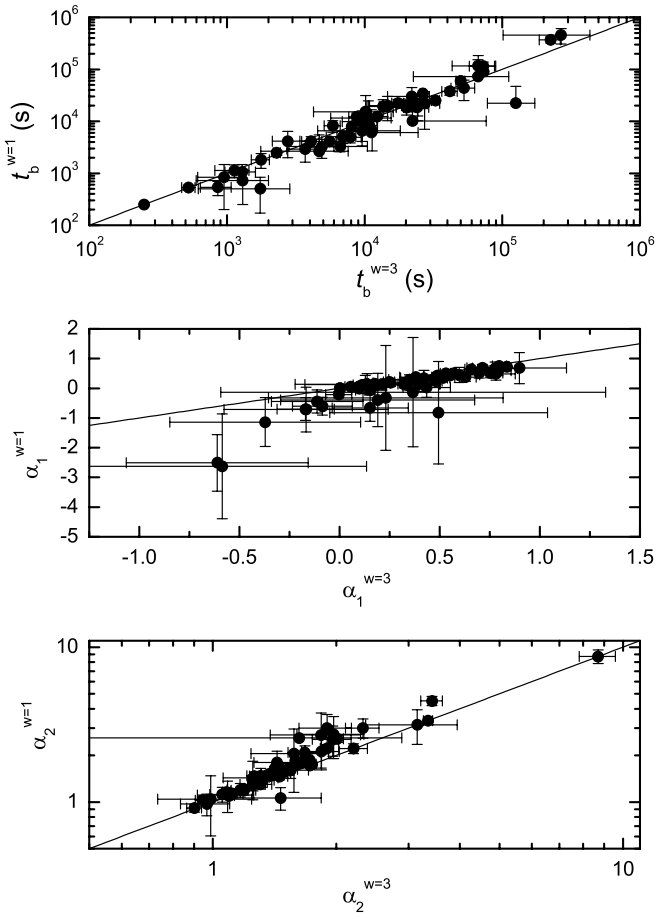

FIG. 1.—Comparison of the fit results for smooth broken power law models with different sharpness parameters, $\omega = 1$ and $\omega = 3$. The diagonal solid lines indicate equality of the two quantities.

of both the prompt and afterglow emission components. The derived α_2 from our fitting with $\omega = 3$ is generally consistent with their results. We therefore fix $\omega = 3$ in this analysis, except for GRBs 060413, 060522, 060607A, and 070710. The XRT light curves of these bursts abruptly drop at t_b, and we take $\omega = 10$. We then create a time filter array that contains two intervals, $[t_1, t_b]$ and $[t_b, t_2]$, for each burst. After specifying this array, we run our code again to extract the spectra in the two intervals and derive their photon indices, $\Gamma_{X,1}$ and $\Gamma_{X,2}$, by fitting the spectra with a power-law model that incorporates absorption by both the Milky Way and the host galaxy, $\texttt{wabs}^{\rm Gal} \times \texttt{zwabs}^{\rm host} \times \texttt{powerlaw}$ (when the redshift is unknown, $\texttt{zwabs}^{\rm host}$ is replaced with the `wabs` model). The $N_{\rm H}^{\rm host}$ in the time-resolved spectral analysis is fixed to the value obtained from fitting the time-integrated spectrum during the entire time span of each burst.

The time t_b is roughly considered to be the duration of the shallow decay phase. As suggested by Lazzati & Begelman (2006) and Kobayashi & Zhang (2007), the zero time of the external-origin power-law segments should be roughly the trigger time from the Burst Alert Telescope (BAT). In our calculation, in order to account for the onset of the afterglow, we take a t_0 that is 10 s after the GRB trigger. The X-ray fluence (S_X) of the shallow decay phase is derived by integrating the fitted light curve from 10 s past the trigger to t_b, without considering the contributions of either early X-ray flares or the GRB tail emissions. Since the shallow decay phase has a temporal decay index shallower than -1, the results are not sensitive to the choice of t_0. We estimate the uncertainty in S_X with a bootstrap method based on the errors in the fitting parameters, $\sigma_{\log F_0}$, $\sigma_{\log t_b}$, σ_{α_1}, and σ_{α_2}, assuming that they are drawn from Gaussian distributions. We generate 5×10^3 parameter sets of (F_0, t_b, α_1, α_2) from the distributions of these parameters for each burst and then calculate S_X for each parameter set. We perform a Gaussian fit to the distribution of $\log S_X$ and derive the central value and its error, $\sigma_{\log S_X}$. In our fits, α_1, t_b, or both are fixed for GRBs 050801 and 060607A. We did not calculate the errors for these two bursts.

We use the following criteria to select our sample: First, the XRT light curves must have a shallow decay segment following the GRB tail. Since the decay slope of the "normal" decay phase predicted by the external GRB models is generally steeper than 0.75, we require that the so-called shallow decay segment have a slope $\alpha_{X,1} < 0.75$ at $1\,\sigma$ error. Second, both the shallow decay segment and the follow-up segment must be bright enough to perform spectral analysis. Systematically going through all the *Swift* XRT data from before 2007 February, we used the above criteria to compile a sample of 53 bursts. Note that the apparently long GRB 060614 is also included in our sample, although it may belong to the class of short-type bursts (Gehrels et al. 2006; Zhang 2006; Zhang et al. 2007a). The XRT light curves and the fitting results are shown in Figure 2, and the data are summarized in Table 1. We collected the BAT observations of these bursts from GCN Circular reports and report them in Table 2. We searched the optical afterglow data on these bursts from published papers and GCN Circulars.[5] We identify a burst as optically bright if three or more detections in the UV-optical band were made. We find that 30 of the 53 bursts are optically bright, but only 15 of these have an optical light curve with good temporal coverage. We corrected for Galactic extinction and converted the observed magnitudes to energy fluxes. We fitted these light curves with a simple power law or the smooth broken power law (ω again fixed at 3). The results are summarized in Table 3. We directly compare the optical data with the XRT data in Figure 2 in order to perform a quick visual check of the achromatism of these light curves. If multiwavelength optical light curves are available, we show only the one that was observed around the X-ray shallow decay phase with the best sampling. Note that the contribution from the host galaxy to the optical light curve of GRB 060614 has been removed.

Twenty-seven of the 53 GRBs in our sample have redshift measurements. Table 4 reports the properties of these bursts in the burst rest frame, including the durations (T'_{90} and t'_b) and the isotropic-equivalent radiation energies ($E_{\rm iso,\gamma}$ and $E_{\rm iso,X}$) in the prompt phase and in the shallow decay phase, and the peak energy of the νf_ν spectrum (E'_p). The $E_{\rm iso,\gamma}$ and $E_{\rm iso,X}$ were calculated as

$$E_{\rm iso,(\gamma,X)} = \frac{4\pi D_L^2 S_{(\gamma,X)}}{1+z}, \qquad (2)$$

where S_γ is the gamma-ray fluence in the BAT band and S_X is the X-ray fluence in the shallow decay phase in the XRT band and where D_L is the luminosity distance of the source. Because of the narrowness of the BAT band, the BAT data cannot well constrain the spectral parameters of GRBs (Zhang et al. 2007b). Generally, the BAT spectrum can be fitted by a simple power law, and the power-law index Γ is correlated with E_p (Zhang et al. 2007a; see also Sakamoto et al. 2007; Cabrera et al. 2007),[6] that is,

$$\log E_p = (2.76 \pm 0.07) - (3.61 \pm 0.26) \log \Gamma. \qquad (3)$$

[5] The GRBlog Web page (http://grad40.as.utexas.edu/grblog.php) was used.

[6] We should point out that this empirical relation is for BAT observations only. The origin of the relation is due to the narrowness of the BAT instrument. It can be robustly used for those bursts whose E_p is roughly within the BAT band.

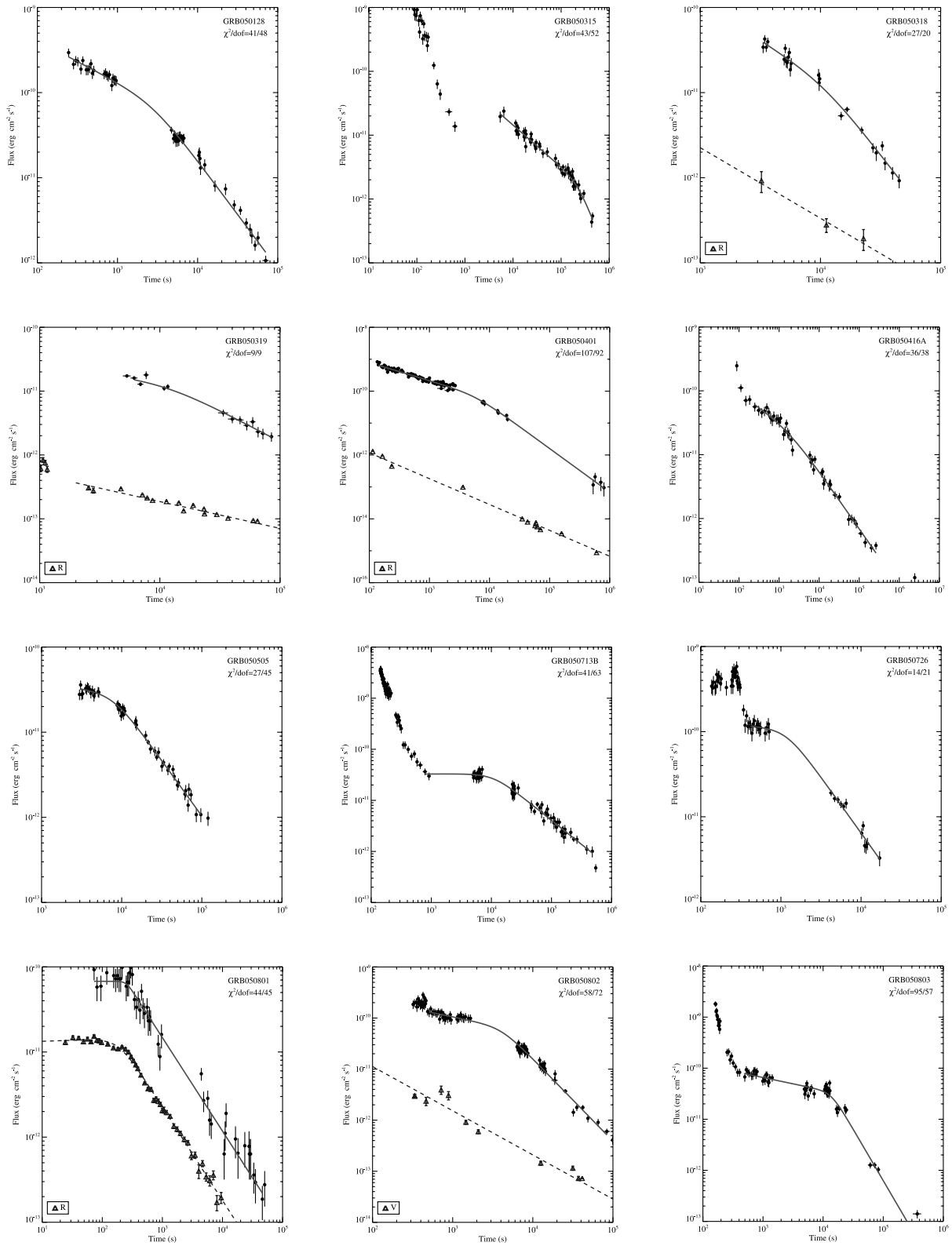

FIG. 2.—XRT light curves (*points*) for the bursts in our sample. The solid lines are the best fits with a smooth broken power law for the shallow decay phase and its subsequent decay phase (usually the ''normal'' decay phase). The χ^2 of the fit and degrees of freedom are shown in each panel. The optical light curves are shown by open triangles, if available. They are fitted with a smooth broken power law or a simple power law (*dashed lines*). [*See the electronic edition of the Journal for a color version of this figure*.]

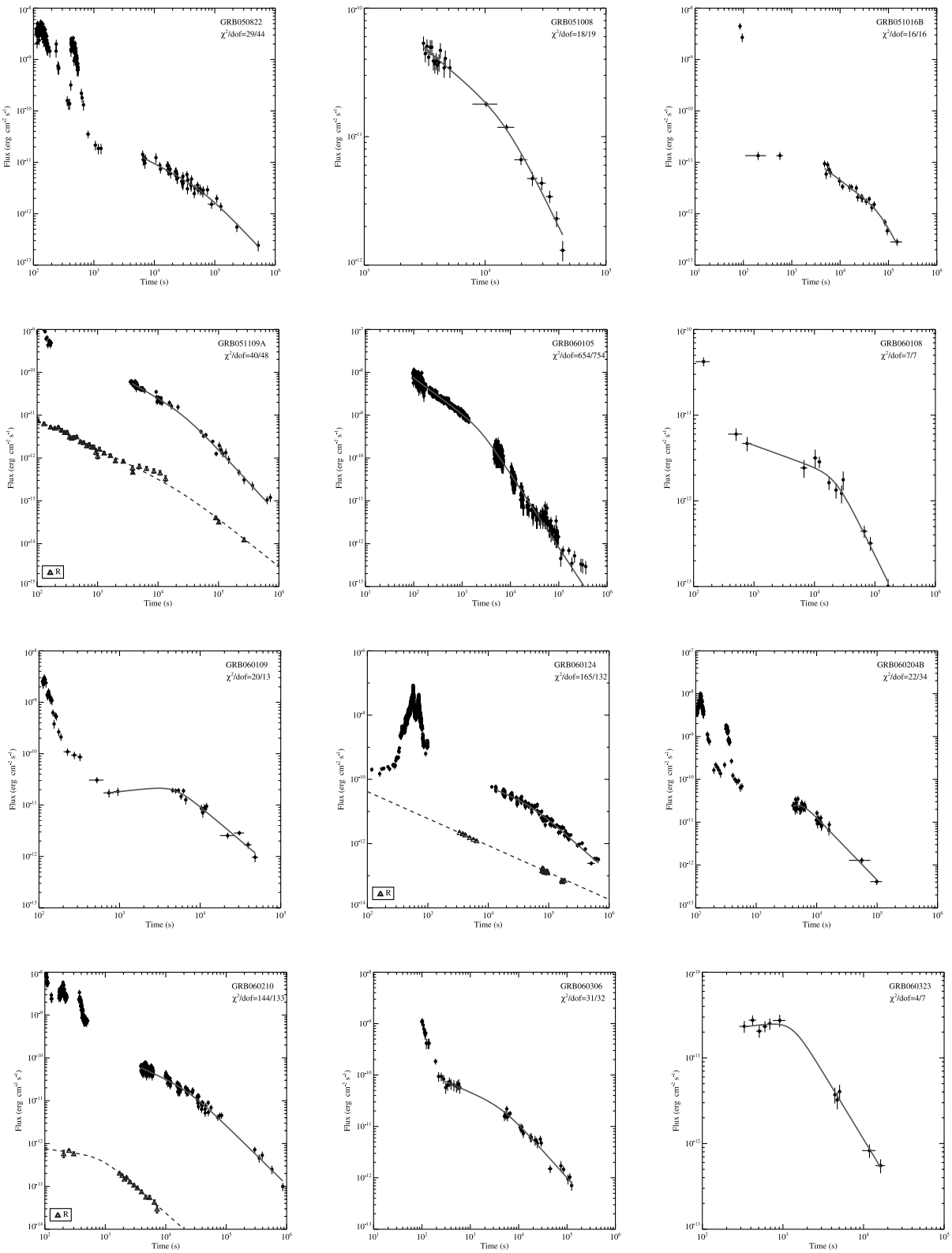

FIG. 2—*Continued*

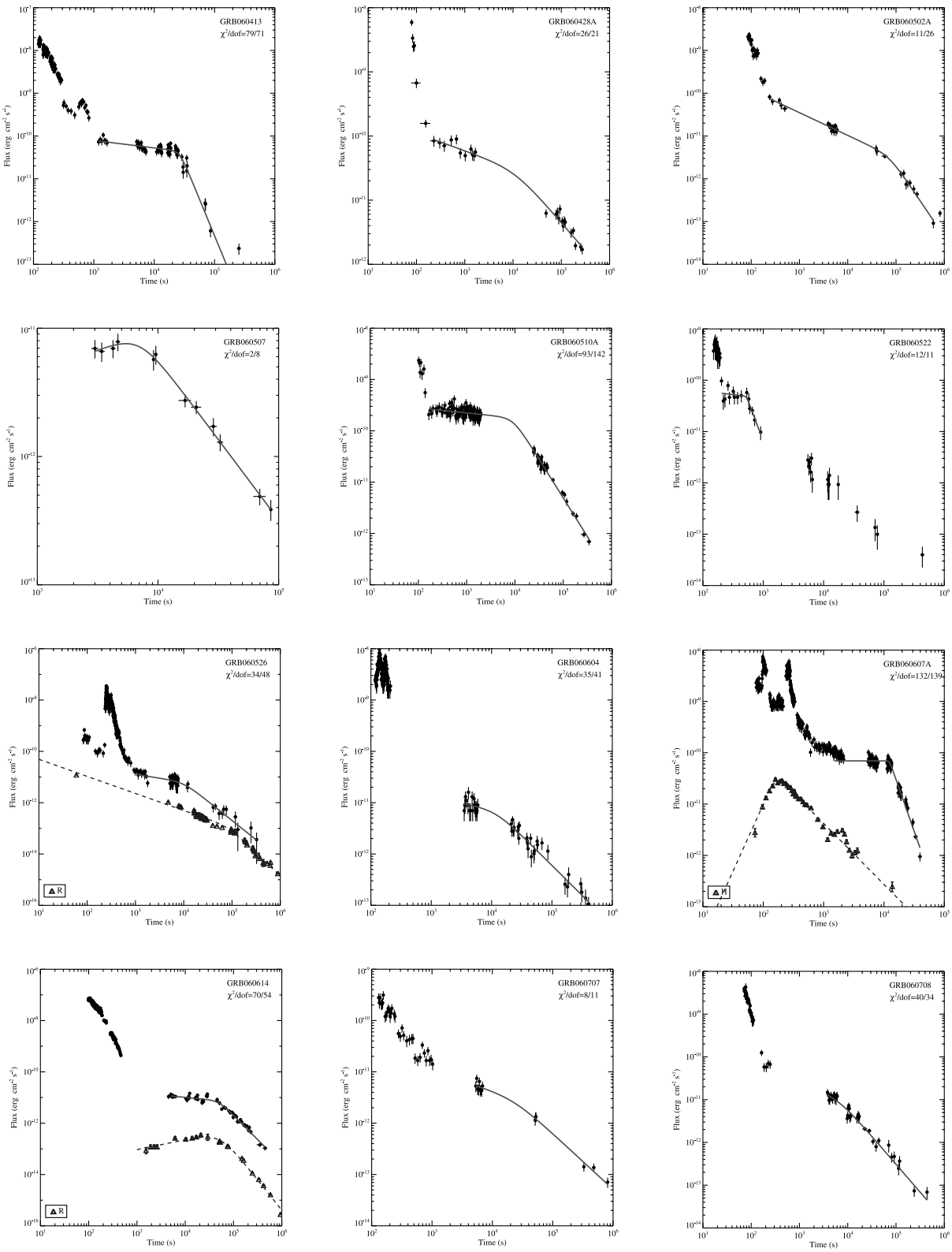

FIG. 2—*Continued*

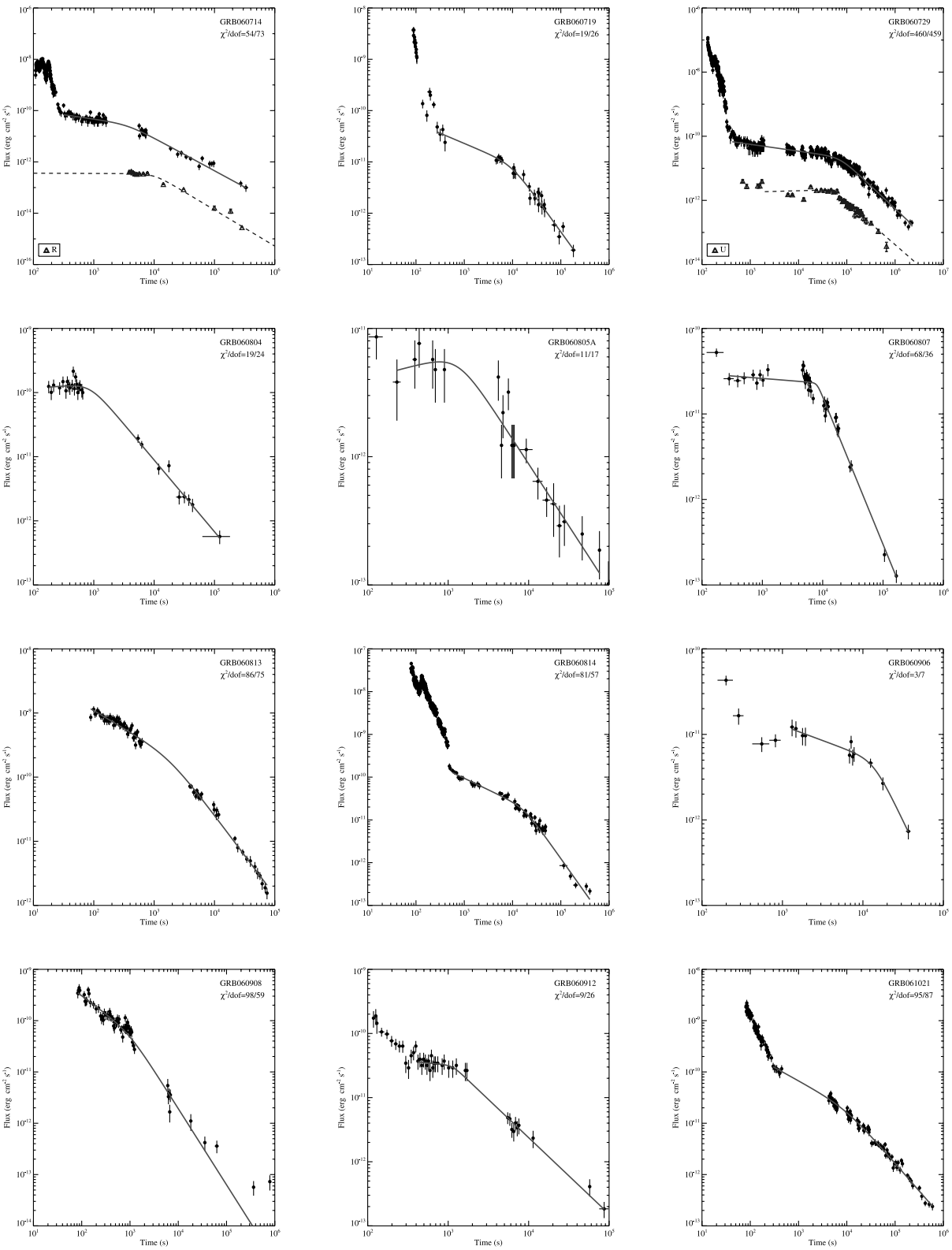

FIG. 2—*Continued*

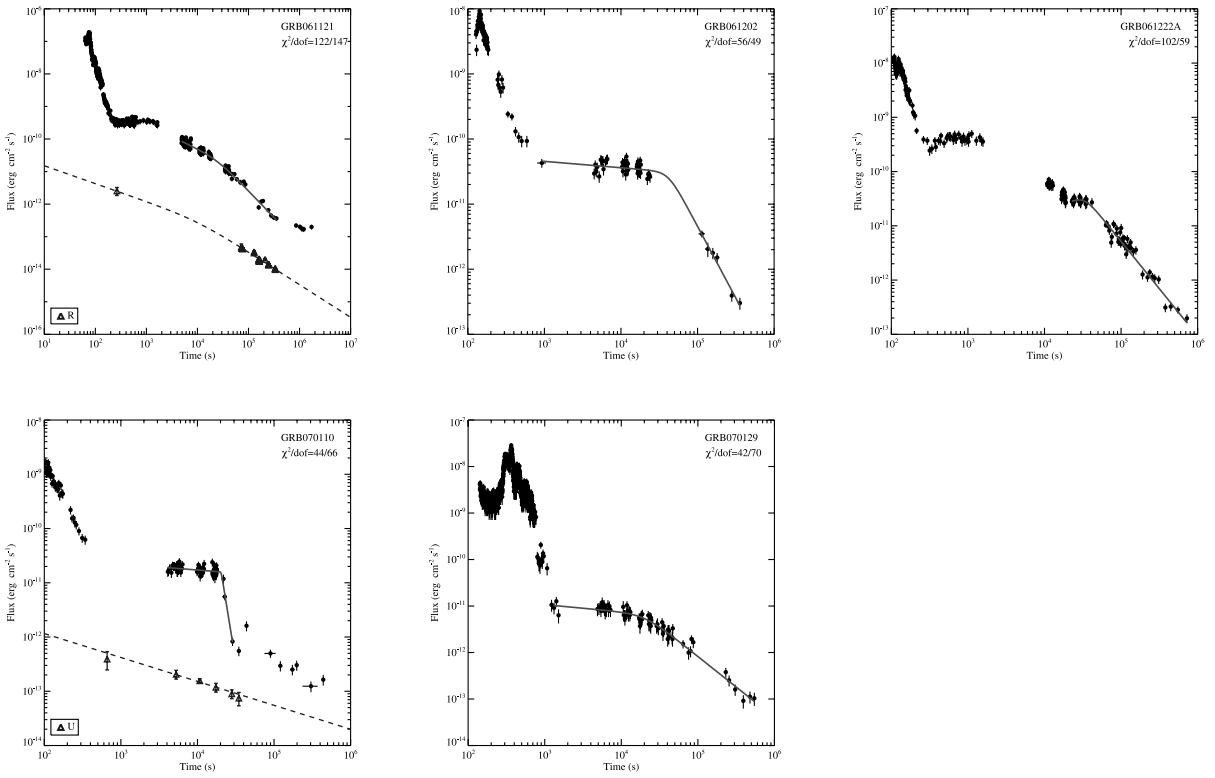

FIG. 2—*Continued*

We estimate E_p with this relation if it is not constrained by the BAT data. We then calculate the *bolometric* energy $E^b_{\rm iso,\gamma}$ in the $1-10^4$ keV band with the *k*-correction method used by Bloom et al. (2001), assuming that the photon indices are -1 and -2.3 before and after E_p, respectively (Preece et al. 2000). Both E'_p and $E^b_{\rm iso,\gamma}$ are listed in Table 4.

3. CHARACTERISTICS OF THE SHALLOW DECAY PHASE AND RELATIONS TO THE PROMPT GAMMA-RAY PHASE

We display the distributions of the characteristics of the shallow decay phase in Figure 3. It is found that these distributions are consistent with being normal or lognormal, that is, $\log t_b({\rm s}) = 4.09 \pm 0.61$, $\log S_{\rm X}({\rm ergs\ cm^{-2}}) = -6.52 \pm 0.69$, $\Gamma_{\rm X,1} = 2.09 \pm 0.21$, and $\alpha_1 = 0.35 \pm 0.35$. Quoted errors are at the 1 σ confidence level.

We next investigate the relationship of the shallow decay phase to the prompt gamma-ray phase. Figure 4 shows t_b, $S_{\rm X}$, $\Gamma_{\rm X,1}$, and $E_{\rm iso,X}$ as functions of T_{90}, S_γ, Γ_γ, and $E_{\rm iso,\gamma}$, respectively. No correlation between Γ_γ and $\Gamma_{\rm X,1}$ is observed. However, $\Gamma_{\rm X,1}$ is larger than Γ_γ except for some X-ray flashes, indicating that the photon spectrum of the shallow decay phase is generally steeper than that of the prompt gamma-ray phase for typical GRBs. It is interesting to note that in contrast to Γ_γ, $\Gamma_{\rm X,1}$ is narrowly clustered around 2.1 (see also O'Brien et al. 2006a), hinting at a possible common microphysical mechanism during the shallow decay phase.

From Figure 4, we find tentative correlations of durations, energy fluences, and isotropic energies between the gamma-ray and X-ray phases. The best fits yield $\log t_b = (0.61 \pm 0.16) \log T_{90} + (3.00 \pm 0.27)$ (Spearman correlation coefficient $r = 0.48$ and $p = 0.003$ for $N = 53$), $\log S_{\rm X} = (0.76 \pm 0.11) \log S_\gamma + (-2.33 \pm 0.60)$ ($r = 0.70$ and $p < 10^{-4}$ for $N = 53$), and $\log E_{\rm iso,X} = (1.00 \pm 0.16) \log E_{\rm iso,\gamma} + (-0.50 \pm 8.10)$ ($r = 0.79$ and $p < 10^{-4}$ for $N = 27$). It is found that t_b weakly depends on T_{90}. However, X-ray fluence and isotropic energy are almost linearly correlated with gamma-ray fluence and gamma-ray energy, respectively. $E_{\rm iso,\gamma}$ is greater than $E_{\rm iso,X}$ for most of the bursts, but in a few cases $E_{\rm iso,X}$ is even larger than $E_{\rm iso,\gamma}$. In order to reveal possible linear correlations for the quantities in the two phases, we define 2 σ linear correlation regions with $y = x + (A \pm 2\sigma_A)$, where y and x are the two quantities in question and A and σ_A are the mean and its 1 σ standard error for the y-x correlation, respectively. The 1 σ regions of the correlations are shown with dashed lines in Figure 4. These results indicate that the radiation during the shallow decay phase is correlated with that in the prompt gamma-ray phase.

4. TESTING THE PHYSICAL ORIGIN OF THE SHALLOW DECAY SEGMENT USING THE PROPERTIES OF THE FOLLOW-UP SEGMENT

The leading scenario for the shallow decay phase is a refreshed forward shock due to either a long-term central engine or a spreading of the ejecta's Lorentz factor (Rees & Mészáros 1998; Dai & Lu 1998a, 1998b; Zhang & Mészáros 2001; Granot & Kumar 2006; Zhang et al. 2006; Nousek et al. 2006; Yu & Dai 2007). Within such a scenario, the shallow decay phase ends at t_b and undergoes a transition to a "normal" decay phase consistent with the standard external forward shock models. Three criteria are required in order to claim the presence of an energy injection break t_b. First, there should be no spectral evolution across t_b, since energy injection is a purely hydrodynamic effect. Second, for the same reason, the break at t_b should be achromatic. Third, the power-law decay phase after t_b should comply with the standard external-shock models. In this section, we test whether all three criteria are satisfied with the data.

Figure 5*a* shows $\Gamma_{\rm X,2}$ as a function of $\Gamma_{\rm X,1}$. The thick solid line is $\Gamma_{\rm X,2} = \Gamma_{\rm X,1}$, and the thin solid lines mark the 3 σ region of the equality, which is defined as $\Gamma_{\rm X,2} = \Gamma_{\rm X,1} + (\mathcal{G} \pm 3\delta_{\mathcal{G}})$, where $\mathcal{G}$ and $\delta_{\mathcal{G}}$ are the mean and statistical uncertainty (1 σ level) of the

TABLE 1

XRT Observations and Fitting Results for Our Sample

GRB	t_1[a] (ks)	t_2[a] (ks)	t_b[b] (ks)	$\alpha_{X,1}$[b]	$\alpha_{X,2}$[b]	χ^2/dof[b]	S_X[c] (10^{-7} ergs cm^{-2})	$\Gamma_{X,1}$[d]	$\Gamma_{X,2}$[d]
050128	0.25	70.72	2.76 ± 0.62	0.49 ± 0.07	1.26 ± 0.03	40/48	3.70 ± 1.07	1.87 ± 0.14	1.95 ± 0.06
050315	5.40	450.87	224.64 ± 38.68	0.66 ± 0.03	1.90 ± 0.28	42/52	10.88 ± 2.56	2.06 ± 0.11	2.18 ± 0.08
050318	3.34	45.19	10.64 ± 4.97	0.90 ± 0.23	1.84 ± 0.19	27/20	5.92 ± 6.32	2.09 ± 0.08	2.02 ± 0.06
050319	6.11	84.79	11.20 ± 13.26	0.23 ± 0.59	0.99 ± 0.25	9/9	1.26 ± 1.42	2.00 ± 0.06	2.04 ± 0.07
050401	0.14	801.04	5.86 ± 0.78	0.57 ± 0.02	1.37 ± 0.06	106/92	9.32 ± 1.31	1.91 ± 0.05	1.99 ± 0.11
050416A	0.25	261.69	1.74 ± 1.12	0.43 ± 0.12	0.90 ± 0.04	36/38	0.62 ± 0.38	2.18 ± 0.31	2.15 ± 0.10
050505	3.07	97.19	7.87 ± 1.57	0.15 ± 0.19	1.30 ± 0.06	26/45	2.34 ± 0.68	2.00 ± 0.07	2.03 ± 0.04
050713B	0.79	478.50	10.80 ± 1.59	-0.00 ± 0.07	0.94 ± 0.04	40/63	3.28 ± 0.35	1.85 ± 0.10	1.94 ± 0.09
050726	0.42	17.05	1.17 ± 0.33	0.08 ± 0.33	1.31 ± 0.09	13/21	1.17 ± 0.53	2.25 ± 0.07	2.07 ± 0.06
050801	0.07	46.10	0.25 (fixed)	0.00 (fixed)	1.10 ± 0.03	44/45	0.16 ± 0.01	1.70 ± 0.19	1.91 ± 0.12
050802	0.51	83.83	4.09 ± 0.61	0.32 ± 0.10	1.61 ± 0.04	58/72	3.66 ± 0.94	1.91 ± 0.06	1.89 ± 0.07
050803	0.50	368.89	13.71 ± 0.90	0.25 ± 0.03	2.01 ± 0.07	94/57	5.96 ± 0.51	1.76 ± 0.14	2.00 ± 0.08
050822	6.41	523.32	66.99 ± 44.38	0.60 ± 0.10	1.25 ± 0.19	29/44	4.05 ± 3.12	2.29 ± 0.13	2.36 ± 0.11
051008	3.09	43.77	14.67 ± 3.82	0.78 ± 0.11	1.96 ± 0.21	17/19	6.87 ± 3.43	2.00 ± 0.11	2.06 ± 0.07
051016B	4.78	150.47	66.40 ± 23.09	0.71 ± 0.08	1.84 ± 0.46	15/16	2.18 ± 1.10	2.15 ± 0.13	2.19 ± 0.13
051109A	3.73	639.16	27.28 ± 7.90	0.79 ± 0.07	1.53 ± 0.08	39/48	10.59 ± 4.71	1.91 ± 0.07	1.90 ± 0.07
060105	0.10	360.83	2.31 ± 0.14	0.84 ± 0.01	1.72 ± 0.02	653/754	42.98 ± 3.84	2.23 ± 0.05	2.15 ± 0.03
060108	0.77	165.26	22.08 ± 7.38	0.26 ± 0.09	1.43 ± 0.17	7/7	0.53 ± 0.17	2.17 ± 0.32	1.75 ± 0.15
060109	0.74	48.01	4.89 ± 1.10	-0.17 ± 0.14	1.32 ± 0.09	19/13	0.91 ± 0.20	2.32 ± 0.15	2.34 ± 0.14
060124	13.30	664.01	52.65 ± 10.33	0.78 ± 0.10	1.65 ± 0.05	165/132	29.65 ± 12.09	2.10 ± 0.03	2.08 ± 0.06
060204B	4.06	98.80	5.55 ± 0.66	-0.59 ± 0.72	1.45 ± 0.07	21/34	0.87 ± 0.36	2.54 ± 0.14	2.77 ± 0.18
060210	3.90	861.94	24.24 ± 5.01	0.63 ± 0.05	1.38 ± 0.05	144/133	10.41 ± 2.90	2.06 ± 0.03	2.12 ± 0.09
060306	0.25	124.39	4.67 ± 2.91	0.40 ± 0.11	1.05 ± 0.07	30/32	1.58 ± 0.98	2.09 ± 0.16	2.21 ± 0.10
060323	0.33	16.28	1.29 ± 0.32	-0.11 ± 0.23	1.55 ± 0.16	4/7	0.27 ± 0.08	1.99 ± 0.16	2.02 ± 0.13
060413	1.20	253.52	26.43 ± 1.12	0.18 ± 0.03	3.42 ± 0.21	78/71	13.77 ± 0.82	1.60 ± 0.08	1.50 ± 0.10
060428A	0.23	271.10	11.04 ± 6.58	0.27 ± 0.09	0.88 ± 0.08	25/21	3.79 ± 1.74	2.11 ± 0.24	2.05 ± 0.14
060502A	0.24	593.06	72.57 ± 15.05	0.53 ± 0.03	1.68 ± 0.15	11/26	5.09 ± 1.19	2.20 ± 0.12	2.15 ± 0.13
060507	3.00	86.09	6.95 ± 1.68	-0.37 ± 0.48	1.25 ± 0.09	2/8	0.40 ± 0.16	2.15 ± 0.19	2.13 ± 0.12
060510A	0.16	343.41	9.18 ± 0.67	0.10 ± 0.03	1.51 ± 0.03	93/142	17.28 ± 1.65	1.91 ± 0.09	1.96 ± 0.06
060522	0.20	0.90	0.53 ± 0.06	0.14 ± 0.36	3.15 ± 0.79	11/11	0.26 ± 0.12	2.03 ± 0.16	2.13 ± 0.30
060526	1.09	322.75	10.02 ± 4.55	0.30 ± 0.12	1.50 ± 0.23	34/48	0.79 ± 0.32	2.08 ± 0.09	2.08 ± 0.16
060604	3.52	403.81	11.37 ± 6.80	0.19 ± 0.48	1.17 ± 0.08	34/41	0.79 ± 0.67	2.44 ± 0.15	2.43 ± 0.17
060607A	1.52	39.52	12.34 ± 0.19	0.00 (fixed)	3.35 ± 0.09	132/139	8.45 ± 0.17	1.44 ± 0.06	1.64 ± 0.05
060614	5.03	451.71	49.84 ± 3.62	0.18 ± 0.06	1.90 ± 0.07	70/54	4.35 ± 0.49	2.02 ± 0.02	1.93 ± 0.06
060707	5.32	813.53	22.21 ± 54.08	0.37 ± 0.96	1.09 ± 0.17	8/11	0.64 ± 2.01	1.88 ± 0.09	2.06 ± 0.20
060708	3.81	439.09	6.66 ± 3.84	0.49 ± 0.54	1.30 ± 0.09	39/34	0.96 ± 1.06	2.41 ± 0.17	2.28 ± 0.12
060714	0.32	331.97	3.70 ± 0.97	0.34 ± 0.10	1.27 ± 0.05	53/73	1.48 ± 0.46	2.15 ± 0.08	2.04 ± 0.11
060719	0.28	182.15	9.57 ± 2.70	0.40 ± 0.06	1.31 ± 0.10	19/26	1.30 ± 0.37	2.35 ± 0.13	2.38 ± 0.26
060729	0.42	2221.24	72.97 ± 3.02	0.21 ± 0.01	1.42 ± 0.02	459/459	19.58 ± 0.83	3.35 ± 0.04	2.26 ± 0.05
060804	0.18	122.07	0.86 ± 0.22	-0.09 ± 0.15	1.12 ± 0.07	18/24	0.97 ± 0.18	2.04 ± 0.23	2.14 ± 0.15
060805A	0.23	75.91	1.30 ± 0.70	-0.17 ± 0.41	0.97 ± 0.13	11/17	0.06 ± 0.03	2.10 ± 0.10	1.97 ± 0.37
060807	0.28	166.22	8.04 ± 0.35	0.06 ± 0.03	1.73 ± 0.05	67/36[e]	1.94 ± 0.11	2.30 ± 0.28	2.22 ± 0.08
060813	0.09	74.25	1.77 ± 0.27	0.55 ± 0.03	1.25 ± 0.03	86/75	7.31 ± 1.36	2.09 ± 0.16	2.04 ± 0.04
060814	0.57	399.37	17.45 ± 1.71	0.54 ± 0.02	1.59 ± 0.05	81/57	6.93 ± 0.87	2.11 ± 0.09	2.30 ± 0.05
060906	1.32	36.69	13.66 ± 3.29	0.35 ± 0.10	1.97 ± 0.36	3/7	0.96 ± 0.29	2.28 ± 0.37	2.12 ± 0.17
060908	0.08	363.07	0.95 ± 0.34	0.70 ± 0.07	1.49 ± 0.09	98/59[e]	1.28 ± 0.61	2.41 ± 0.21	2.00 ± 0.08
060912	0.42	86.80	1.13 ± 0.31	0.13 ± 0.30	1.19 ± 0.08	8/26	0.37 ± 0.15	2.08 ± 0.11	1.95 ± 0.13
061021	0.30	594.16	9.59 ± 2.17	0.52 ± 0.03	1.08 ± 0.03	94/87	3.59 ± 0.87	1.81 ± 0.04	1.70 ± 0.13
061121	4.89	353.10	24.32 ± 4.38	0.75 ± 0.06	1.63 ± 0.05	121/147	19.89 ± 6.14	2.00 ± 0.04	1.93 ± 0.05
061202	0.93	357.04	41.65 ± 5.36	0.10 ± 0.04	2.20 ± 0.18	55/49	13.80 ± 1.12	2.15 ± 0.09	3.55 ± 0.44
061222A	22.78	724.64	32.73 ± 2.17	-0.61 ± 0.45	1.75 ± 0.04	102/59[e]	6.62 ± 1.89	2.46 ± 0.07	2.22 ± 0.12
070110	4.10	28.72	20.40 ± 0.44	0.11 ± 0.05	8.70 ± 0.88	43/66	3.59 ± 0.23	2.16 ± 0.11	2.21 ± 0.09
070129	1.32	546.36	20.12 ± 3.14	0.15 ± 0.07	1.31 ± 0.06	42/70	1.47 ± 0.24	2.25 ± 0.07	2.30 ± 0.10

[a] Start and end times for our light-curve fitting.

[b] Break time and decay slopes before and after the break, and the fit χ^2 (and degrees of freedom).

[c] X-ray fluence of the shallow decay phase, calculated by integrating the fitting light curve from 10 s after the GRB trigger to t_b.

[d] X-ray photon indices before and after t_b.

[e] The fitting results of these bursts have an unacceptable reduced χ^2 due to significant flickering.

TABLE 2

BAT Observations and Redshifts for Our Sample

GRB	T_{90} (s)	S_γ[a] (10^{-7} ergs cm^{-2})	$\Gamma_{\gamma,1}$[b]	$\Gamma_{\gamma,2}$[b]	E_p[b] (keV)	BAT Ref.[c]	z	z Ref.[c]
050128.....	13.8 ± 2.0	45.00 ± 5.00	1.50 ± 0.05	...	133.1 ± 30.2	2992	...	...
050315.....	96.0 ± 10.0	28.00 ± 3.00	1.28 ± 0.00	2.20	37.0 ± 8.0	3105	1.95	3101
050318.....	32.0 ± 2.0	21.00 ± 2.00	2.10 ± 0.11	...	39.5 ± 12.4	3134	1.44	3122
050319.....	10.0 ± 2.0	8.00 ± 0.80	1.25 ± 0.00	2.15	28.0 ± 6.0	3119, Z07	3.24	3136
050401.....	33.0 ± 2.0	140.00 ± 14.00	1.15 ± 0.00	2.65	132.0 ± 16.0	3173, Z07	2.90	3176
050416A.....	2.4 ± 0.2	3.80 ± 0.40	1.00 ± 0.00	3.22	16.0 ± 3.0	3273	0.65	3542
050505.....	60.0 ± 2.0	41.00 ± 4.00	1.50 ± 0.10	...	133.1 ± 41.0	3364, Z07	4.27	3368
050713B.....	75.0 ± 7.5	82.00 ± 10.00	1.00 ± 0.13	...	109.0 ± 32.0	3600, Z07	...	...
050726.....	30.0 ± 3.0	43.00 ± 7.00	1.00 ± 0.16	...	984.0 ± 200.0	3682, Z07	...	...
050801.....	20.0 ± 3.0	4.40 ± 1.00	1.40 ± 0.00	2.00	33.0 ± 7.0	3730, Z07	...	...
050802.....	13.0 ± 2.0	28.00 ± 3.00	1.12 ± 0.00	2.48	118.0 ± 77.0	3737, Z07	1.71	3749
050803.....	110.0 ± 11.0	39.00 ± 3.00	1.05 ± 0.10	...	150.0 ± 68.0	3757, Z07	0.42	3758
050822.....	102.0 ± 2.0	34.00 ± 3.00	1.00 ± 0.00	2.48	36.0 ± 7.0	3856	...	...
051008.....	280.0 ± 28.0	540.00 ± 10.00	0.98 ± 0.09	...	865.0 ± 178.0	4077, Z07	...	...
051016B.....	4.0 ± 0.1	1.70 ± 0.20	2.38 ± 0.23	...	25.2 ± 11.2	4104	0.94	4186
051109A.....	36.0 ± 2.0	21.00 ± 3.00	1.50 ± 0.20	...	133.1 ± 69.0	4217	2.35	4221
060105.....	55.0 ± 5.0	182.00 ± 4.00	1.11 ± 0.03	...	394.8 ± 75.2	4435	...	...
060108.....	14.4 ± 1.0	3.70 ± 0.40	2.01 ± 0.17	...	46.3 ± 18.1	4445	2.03	4539
060109.....	116.0 ± 3.0	6.40 ± 1.00	1.96 ± 0.25	...	50.7 ± 26.3	4476	...	...
060124.....	800.0 ± 10.0	110.00 ± 10.00	1.17 ± 0.27	...	326.5 ± 277.3	4601	2.30	4592
060204B.....	134.0 ± 5.0	30.00 ± 2.00	0.82 ± 0.40	...	96.8 ± 41.0	4671	...	...
060210.....	255.0 ± 10.0	77.00 ± 4.00	1.52 ± 0.09	...	126.9 ± 36.7	4748	3.91	4729
060306.....	61.0 ± 2.0	22.00 ± 1.00	1.85 ± 0.10	...	62.4 ± 18.7	4851	...	...
060323.....	18.0 ± 2.0	5.70 ± 0.60	1.53 ± 0.17	...	124.0 ± 55.3	4912	...	...
060413.....	150.0 ± 10.0	36.00 ± 1.00	1.67 ± 0.08	...	90.4 ± 24.5	4961	...	...
060428A.....	39.4 ± 2.0	14.00 ± 1.00	2.04 ± 0.11	...	43.9 ± 13.8	5022	...	...
060502A.....	33.0 ± 5.0	22.00 ± 1.00	1.43 ± 0.08	...	158.2 ± 43.4	5053	1.51	5052
060507.....	185.0 ± 5.0	45.00 ± 2.00	1.83 ± 0.10	...	64.9 ± 19.3	5091	...	...
060510A.....	21.0 ± 3.0	98.00 ± 5.00	1.55 ± 0.10	...	118.3 ± 36.1	5108	...	...
060522.....	69.0 ± 5.0	11.00 ± 1.00	1.59 ± 0.15	...	107.9 ± 42.7	5153	5.11	5155
060526.....	13.8 ± 2.0	4.90 ± 0.60	1.66 ± 0.20	...	92.3 ± 44.5	5174	3.21	5170
060604.....	10.0 ± 3.0	1.30 ± 0.30	1.90 ± 0.41	...	56.7 ± 46.1	5214	2.68	5218
060607A.....	100.0 ± 5.0	26.00 ± 1.00	1.45 ± 0.07	...	150.5 ± 38.6	5242	3.08	5237
060614.....	102.0 ± 5.0	217.00 ± 4.00	2.13 ± 0.04	...	37.5 ± 9.9	5256	0.125	5275
060707.....	68.0 ± 5.0	17.00 ± 2.00	0.66 ± 0.63	...	66.0 ± 25.0	5289	3.43	5298
060708.....	9.8 ± 1.0	5.00 ± 0.40	1.68 ± 0.12	...	88.4 ± 29.4	5295	...	...
060714.....	115.0 ± 5.0	30.00 ± 2.00	1.99 ± 0.10	...	48.0 ± 14.5	5334	2.71	J06
060719.....	55.0 ± 5.0	16.00 ± 1.00	2.00 ± 0.11	...	47.1 ± 14.7	5349	...	...
060729.....	116.0 ± 10.0	27.00 ± 2.00	1.86 ± 0.14	...	61.2 ± 21.7	5370	0.54	5373
060804.....	16.0 ± 2.0	5.10 ± 0.90	1.78 ± 0.28	...	71.8 ± 43.7	5395	...	...
060805A.....	5.4 ± 0.5	0.74 ± 0.20	2.23 ± 0.42	...	31.8 ± 23.2	5421	...	...
060807.....	34.0 ± 4.0	7.30 ± 0.90	1.57 ± 0.20	...	112.9 ± 56.6	5403	...	...
060813.....	14.9 ± 0.5	55.00 ± 1.00	0.53 ± 0.15	...	192.0 ± 19.0	5443, 5446	...	...
060814.....	146.0 ± 10.0	150.00 ± 2.00	1.56 ± 0.03	...	115.6 ± 24.3	5459	...	...
060906.....	43.6 ± 1.0	22.10 ± 1.40	2.02 ± 0.11	...	45.5 ± 14.2	5538	3.68	5535
060908.....	19.3 ± 0.3	29.00 ± 1.00	1.33 ± 0.07	...	205.5 ± 53.4	5551	2.43	5555
060912.....	5.0 ± 0.5	13.00 ± 1.00	1.74 ± 0.09	...	77.9 ± 22.3	5561	0.94	5617
061021.....	46.0 ± 1.0	30.00 ± 1.00	1.31 ± 0.06	...	217.1 ± 52.4	5744	...	...

TABLE 2—*Continued*

GRB	T_{90} (s)	S_γ[a] (10^{-7} ergs cm^{-2})	$\Gamma_{\gamma,1}$[b]	$\Gamma_{\gamma,2}$[b]	E_p[b] (keV)	BAT Ref.[c]	z	z Ref.[c]
061121.....	81.0 ± 5.0	137.00 ± 2.00	1.41 ± 0.03	...	166.5 ± 33.2	5831	1.31	5826
061202.....	91.0 ± 5.0	35.00 ± 1.00	1.63 ± 0.07	...	98.6 ± 25.4	5887	...	...
061222A.....	72.0 ± 3.0	83.00 ± 2.00	1.39 ± 0.04	...	175.3 ± 36.8	5964	...	...
070110.....	85.0 ± 5.0	16.00 ± 1.00	1.57 ± 0.12	...	112.9 ± 38.4	6007	2.35	6010
070129.....	460.0 ± 20.0	31.00 ± 3.00	2.05 ± 0.16	...	43.1 ± 16.1	6058	...	...

[a] Observed gamma-ray fluence and its error in the 15–150 keV band.

[b] The spectrum of the prompt gamma rays is generally fitted by a simple power law, $f_\nu \propto \nu^{-\Gamma_{\gamma,1}}$. We estimate the E_p for these bursts with the empirical relation between Γ_{γ_1} and E_p for the BAT observations. A few cases are fitted with a cutoff power law or the Band function (the photon indices before and after the break energy are $\Gamma_{\gamma,1}$ and $\Gamma_{\gamma,2}$, respectively).

[c] References for BAT and redshift data.

REFERENCES.—(J06) Jakobsson et al. 2006c; (Z07) Zhang et al. 2007b; (2992) Cummings et al. 2005; (3101) Kelson & Berger 2005; (3105) Krimm et al. 2005a; (3119) Krimm et al. 2005b; (3122) Berger & Mulchaey 2005; (3134) Krimm et al. 2005c; (3136) Fynbo et al. 2005a; (3173) Sakamoto et al. 2005a; (3176) Fynbo et al. 2005b; (3273) Sakamoto et al. 2005c; (3364) Hullinger et al. 2005a; (3368) Berger et al. 2005; (3542) Cenko et al. 2005; (3600) Parsons et al. 2005a; (3682) Barthelmy et al. 2005a; (3730) Sakamoto et al. 2005b; (3737) Palmer et al. 2005; (3749) Fynbo et al. 2005c; (3757) Parsons et al. 2005b; (3758) Bloom et al. 2005; (3856) Hullinger et al. 2005b; (4077) Barthelmy et al. 2005b; (4104) Barbier et al. 2005; (4186) Soderberg et al. 2005; (4217) Fenimore et al. 2005; (4221) Quimby et al. 2005; (4435) Markwardt et al. 2006a; (4445) Sakamoto et al. 2006a; (4476) Palmer et al. 2006a; (4539) Melandri et al. 2006; (4592) Cenko et al. 2006a; (4601) Lamb et al. 2006; (4671) Markwardt et al. 2006b; (4729) Cucchiara et al. 2006a; (4748) Sakamoto et al. 2006b; (4851) Hullinger et al. 2006; (4912) Parsons et al. 2006a; (4961) Barbier et al. 2006b; (5022) Markwardt et al. 2006c; (5052) Cucchiara et al. 2006b; (5053) Parsons et al. 2006b; (5091) Barbier et al. 2006a; (5108) Barbier et al. 2006c; (5153) Krimm et al. 2006a; (5155) Cenko et al. 2006b; (5170) Berger & Gladders 2006; (5174) Markwardt et al. 2006d; (5214) Parsons et al. 2006c; (5218) Castro-Tirado et al. 2006; (5237) Ledoux et al. 2006; (5242) Tueller et al. 2006a; (5256) Barthelmy et al. 2006a; (5275) Price et al. 2006; (5289) Stamatikos et al. 2006a; (5295) Fenimore et al. 2006a; (5298) Jakobsson et al. 2006b; (5334) Krimm et al. 2006b; (5349) Sakamoto et al. 2006c; (5370) Parsons et al. 2006d; (5373) Thöne et al. 2006; (5395) Tueller et al. 2006b; (5403) Barbier et al. 2006d; (5421) Barthelmy et al. 2006b; (5443) Cummings et al. 2006; (5446) Golenetskii et al. 2006; (5459) Stamatikos et al. 2006b; (5535) Vreeswijk et al. 2006; (5538) Sato et al. 2006; (5551) Palmer et al. 2006c; (5555) Rol et al. 2006; (5561) Parsons et al. 2006e; (5617) Jakobsson et al. 2006a; (5744) Palmer et al. 2006b; (5826) Bloom et al. 2006; (5831) Fenimore et al. 2006b; (5887) Sakamoto et al. 2006d; (5964) Tueller et al. 2006c; (6007) Cummings et al. 2007; (6010) Jaunsen et al. 2007; (6058) Krimm et al. 2006c.

difference $\Gamma_{X,2} - \Gamma_{X,1}$. Note that $\delta_{\mathcal{G}}$ does not include the observational uncertainty. It statistically describes the scatter of $\mathcal{G}$ for the bursts in our sample. We find that only one burst, GRB 061202, is out of this region. A comparison between the distributions of $\Gamma_{X,2}$ and $\Gamma_{X,1}$ is shown in Figure 5*b*. Excluding GRB 061202, the two distributions are consistent. The Kolmogorov-Smirnov test suggests that the significance level of this consistency is 0.96. These results indicate that $\Gamma_{X,1}$ and $\Gamma_{X,2}$ for the bursts in our sample are globally consistent with each other. In order to verify this consistency within the observational uncertainty for individual bursts, Figure 5*c* shows the distribution of the ratio $\mu = \mathcal{G}/\sigma$, where $\sigma^2 = \delta\Gamma^2_{X,1} + \delta\Gamma^2_{X,2}$ is the observed uncertainty of $\mathcal{G}$.

TABLE 3

OPTICAL OBSERVATIONS AND FITTING RESULTS

GRB	t_1[a] (ks)	t_2[a] (ks)	$t_{b,o}$[b] (ks)	$\alpha_{o,1}$[b]	$\alpha_{o,2}$[b]	χ^2/dof[b]	References
050318.....	3.23	22.83	...	0.84 ± 0.22	...	0.5/1	1
050319.....	2.00	204.74	...	0.42 ± 0.02	...	11/16	2–4
050401.....	0.06	1231.18	...	0.80 ± 0.01	...	43/12	5–7
050801.....	0.02	9.49	0.19 ± 0.02	−0.02 ± 0.07	1.10 ± 0.02	26/42	8
050802.....	0.34	127.68	...	0.85 ± 0.02	...	50/10	9–11
051109A.....	0.04	20170.00	21.80 ± 10.95	0.66 ± 0.02	1.10 ± 0.08	106/42	12
060124.....	3.34	1979.30	...	0.85 ± 0.02	...	11/19	13–14
060210.....	0.09	7.19	0.70 ± 0.18	0.01 ± 0.24	1.23 ± 0.08	5/12	15–16
060526.....	0.06	893.55	84.45 ± 5.88	0.67 ± 0.02	1.80 ± 0.04	116/56	17
060607A.....	0.07	13.73	0.16 (fixed)	−3.07 ± 0.25	1.18 ± 0.02	92/35	18
060614.....	1.54	934.36	39.09 ± 1.71	−0.40 ± 0.05	2.16 ± 0.03	114/24	19–21
060714.....	3.86	285.87	1.00 (fixed)	0.01 (fixed)	1.41 ± 0.03	35/11	22–26
060729.....	20.00	662.39	43.29 ± 5.15	−0.37 ± 0.34	1.34 ± 0.06	36/27	27
061121.....	0.26	334.65	1.70 ± 0.73	0.17 (fixed)	0.99 ± 0.05	18/23	28
070110.....	0.66	34.76	...	0.43 ± 0.08	...	1/4	29

[a] Time interval concerned in our fitting.

[b] For a smooth broken power law fit, $t_{b,o}$, $\alpha_{o,1}$, and $\alpha_{o,2}$ are the break time and the decay slopes before and after the break. For a simple power-law fit, the decay index and its error are shown in column "$\alpha_{o,1}$." In order to make the fits more reasonable, we assume an error of 0.1 mag for those data points without observational errors available.

REFERENCES.—(1) Still et al. 2005; (2) Quimby et al. 2006; (3) Huang et al. 2007; (4) Mason et al. 2006; (5) De Pasquale 2006; (6) Rykoff et al. 2005; (7) Watson et al. 2006; (8) Rykoff et al. 2006; (9) McGowan et al. 2005b; (10) Pavlenko et al. 2005; (11) McGowan et al. 2005a; (12) Yost et al. 2007; (13) Misra et al. 2007; (14) Romano et al. 2006; (15) Curran et al. 2007; (16) Stanek et al. 2007; (17) Dai et al. 2007; (18) Molinari et al. 2007; (19) Fynbo et al. 2006; (20) Della Valle et al. 2006; (21) Gal-Yam et al. 2006; (22) Asfandyarov et al. 2006; (23) Rumyantsev et al. 2006; (24) Pavlenko et al. 2006b; (25) Jakobsson et al. 2006c; (26) Pavlenko et al. 2006a; (27) Grupe et al. 2007; (28) Page et al. 2007; (29) Troja et al. 2007.

TABLE 4
Rest-Frame Properties of the Bursts with Known Redshifts in Our Sample

GRB	$\log T'_{90}$(s)	$\log E'_p$(keV)	$\log E_{\rm iso,\gamma}$(ergs)	$\log E^b_{\rm iso,\gamma}$(ergs)	$\log E_{\rm iso,X}$(ergs)	$\log t'_b$(s)
050315	1.51 ± 0.05	2.0 ± 0.1	52.41 ± 0.05	52.84	51.94 ± 0.10	4.83 ± 0.07
050318	1.12 ± 0.03	2.0 ± 0.1	52.04 ± 0.04	52.38	51.88 ± 0.46	4.03 ± 0.20
050319	0.37 ± 0.09	2.1 ± 0.1	52.24 ± 0.04	52.69	52.03 ± 0.49	4.01 ± 0.51
050401	0.93 ± 0.03	2.7 ± 0.1	53.41 ± 0.04	53.69	52.82 ± 0.06	3.77 ± 0.06
050416A	0.16 ± 0.04	1.4 ± 0.1	50.62 ± 0.05	51.00	49.69 ± 0.26	2.88 ± 0.28
050505	1.06 ± 0.01	2.8 ± 0.1	53.14 ± 0.04	53.51	52.62 ± 0.13	3.90 ± 0.09
050802	0.68 ± 0.07	2.5 ± 0.3	52.31 ± 0.05	52.62	51.86 ± 0.11	3.61 ± 0.06
050803	1.89 ± 0.04	2.3 ± 0.2	51.24 ± 0.03	51.67	50.29 ± 0.04	3.85 ± 0.03
051016B	0.32 ± 0.01	1.7 ± 0.2	50.59 ± 0.05	50.95	50.99 ± 0.22	4.82 ± 0.15
051109A	1.03 ± 0.02	2.6 ± 0.2	52.43 ± 0.06	52.82	52.65 ± 0.19	4.44 ± 0.13
060108	0.68 ± 0.03	2.1 ± 0.2	51.56 ± 0.05	51.89	51.20 ± 0.14	4.34 ± 0.15
060124	2.38 ± 0.01	3.0 ± 0.4	53.13 ± 0.04	53.72	53.08 ± 0.18	4.72 ± 0.09
060210	1.72 ± 0.02	2.8 ± 0.1	53.36 ± 0.02	53.72	53.18 ± 0.12	4.38 ± 0.09
060502A	1.12 ± 0.07	2.6 ± 0.1	52.10 ± 0.02	52.54	51.82 ± 0.10	4.81 ± 0.09
060522	1.05 ± 0.03	2.8 ± 0.2	52.69 ± 0.04	53.03	51.29 ± 0.19	2.16 ± 0.05
060526	0.52 ± 0.06	2.6 ± 0.2	52.02 ± 0.05	52.36	51.21 ± 0.26	3.38 ± 0.25
060604	0.43 ± 0.13	2.3 ± 0.4	51.32 ± 0.10	51.64	50.88 ± 0.37	3.27 ± 0.26
060607A	1.39 ± 0.02	2.8 ± 0.1	52.72 ± 0.02	53.12	52.84 ± 0.01	4.09 ± 0.01
060614	1.96 ± 0.02	1.6 ± 0.1	50.90 ± 0.01	51.24	49.25 ± 0.05	4.70 ± 0.03
060707	1.19 ± 0.03	2.5 ± 0.2	52.61 ± 0.05	52.98	51.44 ± 1.36	3.95 ± 1.06
060714	1.49 ± 0.02	2.3 ± 0.1	52.69 ± 0.03	53.01	51.95 ± 0.14	3.57 ± 0.11
060729	1.88 ± 0.04	2.0 ± 0.2	51.31 ± 0.03	51.65	51.35 ± 0.02	4.86 ± 0.02
060906	0.97 ± 0.01	2.3 ± 0.1	52.78 ± 0.03	53.09	51.57 ± 0.13	3.62 ± 0.10
060908	0.75 ± 0.01	2.8 ± 0.1	52.59 ± 0.01	53.07	51.12 ± 0.21	2.32 ± 0.16
060912	0.41 ± 0.04	2.2 ± 0.1	51.47 ± 0.03	51.83	50.21 ± 0.17	3.05 ± 0.12
061121	1.54 ± 0.03	2.6 ± 0.1	52.78 ± 0.01	53.23	51.83 ± 0.13	3.90 ± 0.08
070110	1.40 ± 0.03	2.6 ± 0.1	52.31 ± 0.03	52.68	52.19 ± 0.03	4.31 ± 0.01

A positive value of μ would indicate a hard-to-soft spectral evolution. This ratio indicates the significance level of the difference between $\Gamma_{X,1}$ and $\Gamma_{X,2}$ for individual bursts within the observational uncertainties of the two quantities. As shown in Figure 5*c*, most of the bursts ($\sim$90%) have $\mu \lesssim 1$, and only one burst (GRB 061202) has $\mu > 3$. These results prove that no significant spectral evolution between the two phases with a confidence level above 3 σ is observed for the bursts in our sample within the observational error, except for GRB 061202. This is consistent with the expectation from refreshed-shock afterglow models. Note that GRB 061202 shows significant hard-to-soft spectral evolution from the shallow to the normal decay phase, that is, from $\Gamma_{X,1} = 2.25 \pm 0.07$ to $\Gamma_{X,2} = 3.55 \pm 0.44$. One caveat to this spectral evolution is that there is a long observational gap between the first epoch in the shallow decay phase (4×10^3 to 2×10^4 s) and the second epoch in normal decay phase (1×10^5 to 5×10^5 s) in which the spectral indices are measured. Without detecting the break itself, it may be dangerous to draw the conclusion that spectral variation is clearly seen across t_b. We cannot rule out the possibility that the plateau extends further and drops dramatically before landing on a normal decay segment as is seen in GRBs 060522 and 070110 (see discussion below).

Although the mechanism of energy injection into the forward shock could vary (e.g., Rees & Mészáros 1998; Dai & Lu 1998a, 1998b; Zhang & Mészáros et al. 2001; Yu & Dai 2007), the kinetic energy of the fireball once the energy injection is complete should be constant, and this "normal" decay phase should be explainable with the standard external-shock models. Without broadband afterglow modeling, the "closure relations" between the observed spectral index β and temporal decay index α present a simple test of the models. In Figure 6, we present $\alpha_{X,2}$ as a function of spectral index $\beta_{X,2}$, where $\beta_{X,2} = \Gamma_{X,2} - 1$. The closure correlations of the external-shock afterglow models for different spectral regimes, different cooling schemes, different properties of the ambient medium, and different electron distributions (spectral index $p > 2$ and $p < 2$) are shown in Figure 6 (see Table 1 of Zhang & Mészáros 2004 and references therein [in particular, Sari et al. 1998; Chevalier & Li 2000; Dai & Cheng 2001]). The fact that the observed $\beta_{X,2}$ is greater than 0.5 for the bursts in our sample suggests that these X-rays are in the spectral regime $\nu_X > \max(\nu_m, \nu_c)$ (regime I) or $\nu_m < \nu_X < \nu_c$ (regime II), where ν_m and ν_c are the characteristic frequency and cooling frequency of synchrotron radiation, respectively. The relation between α and β for spectral regime I is $\alpha = (3\beta - 1)/2$ regardless of the type of medium (interstellar [ISM] or wind). If the X-ray band is in regime II, we have $\alpha = 3\beta/2$ (for ISM) and $\alpha = (3\beta + 1)/2$ (for wind). We define

$$D = |\alpha^{\rm obs} - \alpha(\beta^{\rm obs})|,$$
$$\delta_D = \sqrt{(\delta\alpha^{\rm obs})^2 + [\delta\alpha(\beta^{\rm obs})]^2}, \quad (4)$$

where $\alpha^{\rm obs}$ and $\alpha(\beta^{\rm obs})$ are the temporal decay slopes from the observations and from the closure relations, respectively, and $\delta\alpha^{\rm obs}$ and $\delta\alpha(\beta^{\rm obs})$ are their errors. The ratio $\phi = D/\delta_D$ reflects the "nearness" of the data point to the model predictions within the error scope. If $\phi < 1$, we consider that the data point goes across the corresponding closure relation line. If $\phi < 3$, we conclude that the model cannot be excluded within 3 σ significance. Those bursts that have large uncertainties on both α and β may be interpreted with more than one model. In this case, we compare ϕ-values derived from these models and take the model that gives the smallest ϕ.

As shown in Figure 6, 24 out of the 53 bursts distribute around the line for spectral regime I. A group of these have a decay slope shallower than the model prediction, but they are slightly below and almost keep abreast with the regime I model line (see also

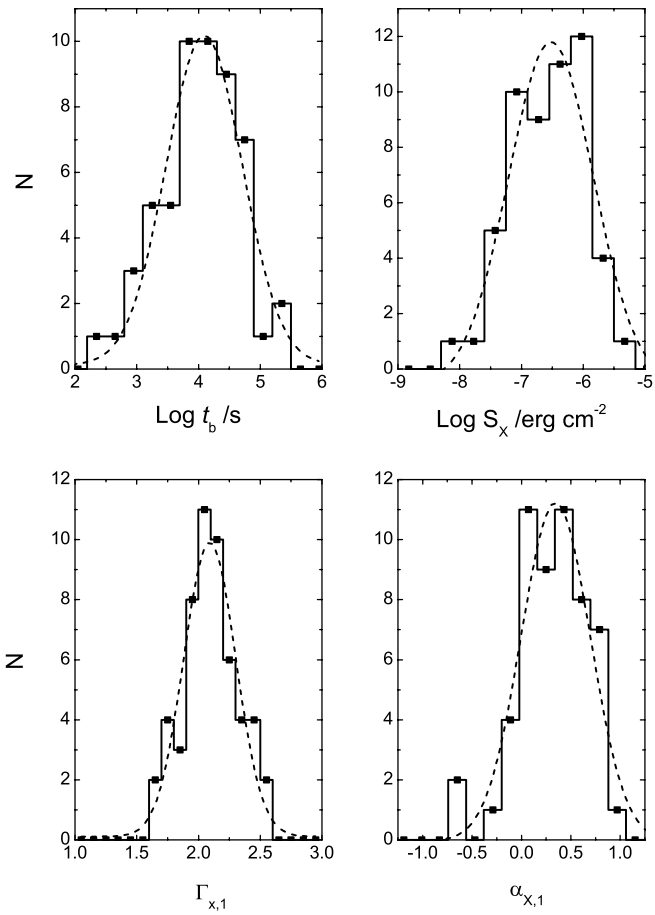

FIG. 3.—Distributions of the characteristics of the shallow decay segment for the bursts in our sample. The dashed lines are the results of Gaussian fits.

Fig. 5 of Willingale et al. 2007). At the 3 σ confidence level, this model cannot be excluded for these bursts. Eighteen bursts are consistent with the ISM external-shock afterglow model in spectral regime II.

Six bursts (GRBs 050315, 050318, 050803, 060614, 051008, and 060906) agree with both the regime I ISM jet model and the regime II wind model. The observed β's of these six bursts are $\sim$1. The two models are almost degenerate at $\beta \sim 1$. We therefore use the spectral and temporal behaviors of the prior segment to distinguish the two models. Since the observed $\beta > 0.5$ in our sample, the decay slope of the light curves before a jet break should be steeper than $3\beta/2 \sim 0.75$. From Table 1, we can see that the α_1-values are 0.66 ± 0.03, 0.90 ± 0.23, 0.25 ± 0.03, 0.18 ± 0.06, 0.78 ± 0.11, and 0.35 ± 0.10, respectively, for the six bursts. So, there is no firm evidence to claim a jet break within the uncertainty of the decay slope for these bursts.[7] Since in the energy injection model the shallow decay slope depends on a free parameter q, we tentatively suggest that these six cases can be explained with a wind afterglow model in spectral regime II. GRB 060108 is also consistent with this model according to our criterion.

As shown above, the spectral index and temporal decay slope of the normal decay phase for most bursts in our sample (49 out of 53 bursts) are roughly consistent with the closure relations of the external-shock models. This further favors the idea that the shallow decay segment is also of external-shock origin and probably is related to a long-term energy injection effect. In this scenario, the energy injection break should be achromatic, if the multiple wavelengths of radiation are all from the same emission region, presumably the forward shock. We therefore inspect the optical light curves of these bursts to examine whether the breaks observed in the XRT light curves are achromatic. Among these, 13 bursts have well-sampled optical light curves, as shown in Figure 2 and Table 3. The optical light curves of GRBs 050801, 051109A, 060614, 060714, 060729, and 061121 show a break around t_b, indicating that the breaks in both the X-ray and the optical bands are consistent with being achromatic. However, the optical light curves of GRBs 050318, 050319, 050802, 060124, and 050401 do not have a break around t_b (see also Panaitescu et al. 2006a). They can be well fitted by a simple power-law model. GRBs 060210 and 060526 have an optical break, but the breaks are not around t_b.

GRBs 060413, 060522, 060607A, and 070110 have a plateau with a steplike, sharp drop ($\omega = 10$ is required in our data fitting). Aside from GRB 060522, the other three bursts deviate significantly from any external-shock afterglow model at the 3 σ significance level. Although the sharp-drop segment of GRB 060522 is consistent with the regime II, wind-jet model, the plateau convincingly rules out this model, since it cannot be explained as the prejet segment within the same model. These results suggest that the sharp-drop segment and its prior plateau in these bursts are very likely not of external-shock origin. A direct support of this speculation is that the optical light curves of these bursts, where available, all evolve independently with respect to the X-ray light curves. For example, the optical light curve of GRB 060607A rapidly increases (with $F \propto t^3$) up to a maximum at $t = 160$ s after the GRB trigger and then continuously decays with an index of -1.18 ± 0.02 (Molinari et al. 2007). The X-ray light curve, on the other hand, shows significant flares before 600 s and a plateau lasting from 600 to $\sim 1.2 \times 10^4$ s after the GRB trigger. At the end of the plateau, the XRT light curve drops sharply, with $\alpha_2 = 3.35 \pm 0.09$. During the plateau in the XRT light curve, the optical light curve "normally" decays until the occurrence of a significant flare around 2000 s. The optical light curve is consistent with an external forward shock, and the peak is consistent with onset of the afterglow (Molinari et al. 2007). The plateau and the sharp drop in the XRT light curve of GRB 070110 are similar to those of GRB 060607A, but an additional "normal" decay component past the steep falloff was also observed (Troja et al. 2007). The decay slope of this late X-ray emission component is similar to that of the optical light curve and is likely of external-shock origin (cf. also GRB 060522). This reinforces the suggestion that the early X-ray plateau is of internal origin and is connected to a long-lasting central engine (Troja et al. 2007). A common signature of these internal-origin plateaus is that the flux remains nearly constant on the plateau, but with significant flickering. Although it may not be unreasonable to interpret this as late internal shocks (which usually give rise to erratic collisions within the ejecta and may power X-ray flares), another possibility

[7] The possibility that a jet break is coincident with an energy injection break is however not ruled out. The normal decay phase could be missed in data fitting, if the normal decay segment is short, the data are sparse, or the jet break is not significant (e.g., Wei & Lu 2000; Kumar & Panaitescu 2000a; Gou et al. 2001). One example of this scenario is GRB 060614. Our best fit with a smooth broken power law does not reveal a jetlike break from a normal decay phase. However, Mangano et al. (2007) suggest a normal decay phase between 3.66×10^4 and 1.04×10^5 s by fitting the light curve with a joint power law model (the breaks are guided by eye). They showed that the decay slope during this period is 1.03 ± 0.02. This normal decay phase thus satisfies a closure relation of standard forward-shock models. For a detailed study of jet breaks, see Paper III in this series (Liang et al. 2007).

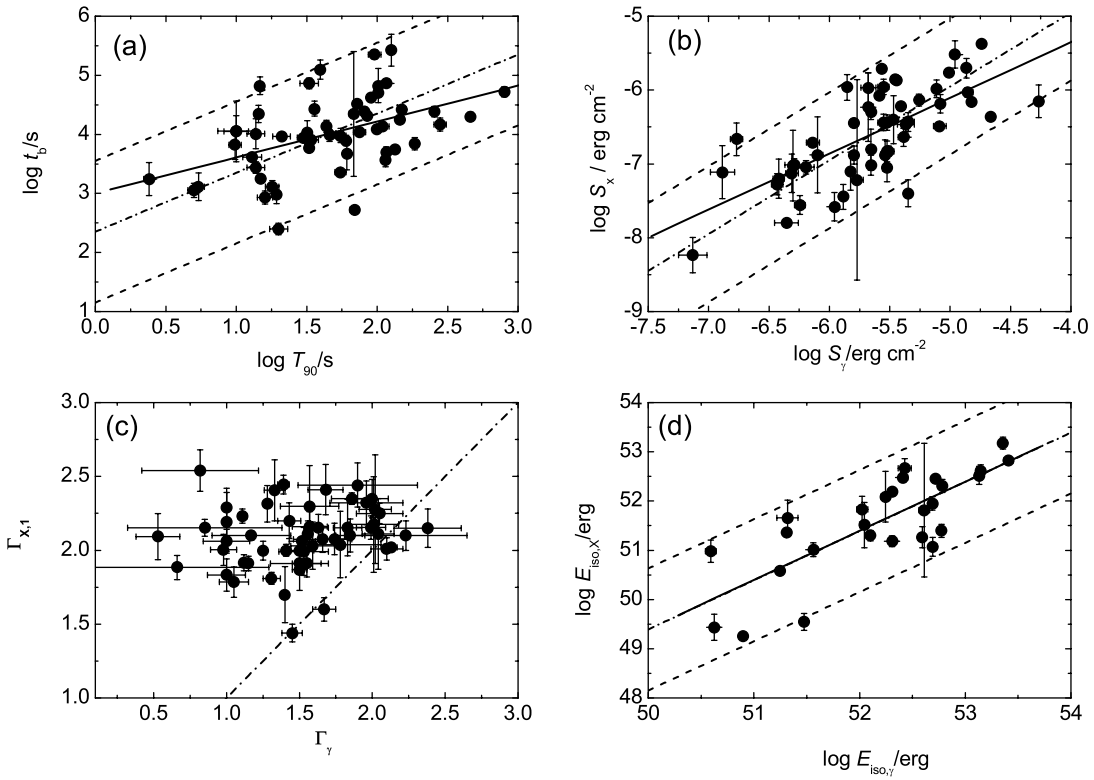

FIG. 4.—Correlations between the data for the shallow decay phase and the prompt gamma-ray phase. The solid lines in (*a*), (*b*), and (*d*) are the best fit. The dashed lines mark a 2 σ region defined as $y = x + (A \pm 2\sigma_A)$, where y and x are the quantities on the y- and x-axes, respectively, and A and σ_A are the mean and its 1 σ standard error for the y-x correlation, respectively. The dash-dotted lines show $y = x$.

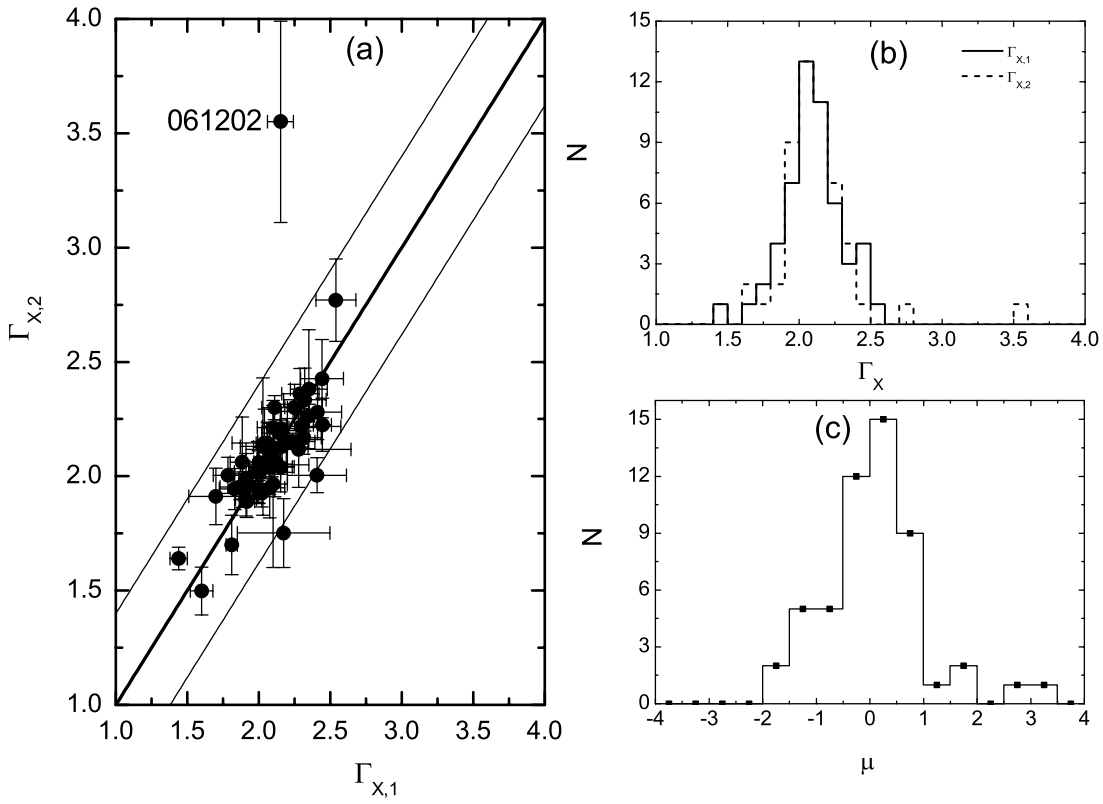

FIG. 5.—Comparison between $\Gamma_{X,1}$ and $\Gamma_{X,2}$. (*a*) $\Gamma_{X,1}$ vs. $\Gamma_{X,2}$. The solid lines mark the equality $\Gamma_{X,2} = \Gamma_{X,1}$ and its 2 σ region. (*b*) Histograms of $\Gamma_{X,1}$ and $\Gamma_{X,2}$. (*c*) Distribution of μ.

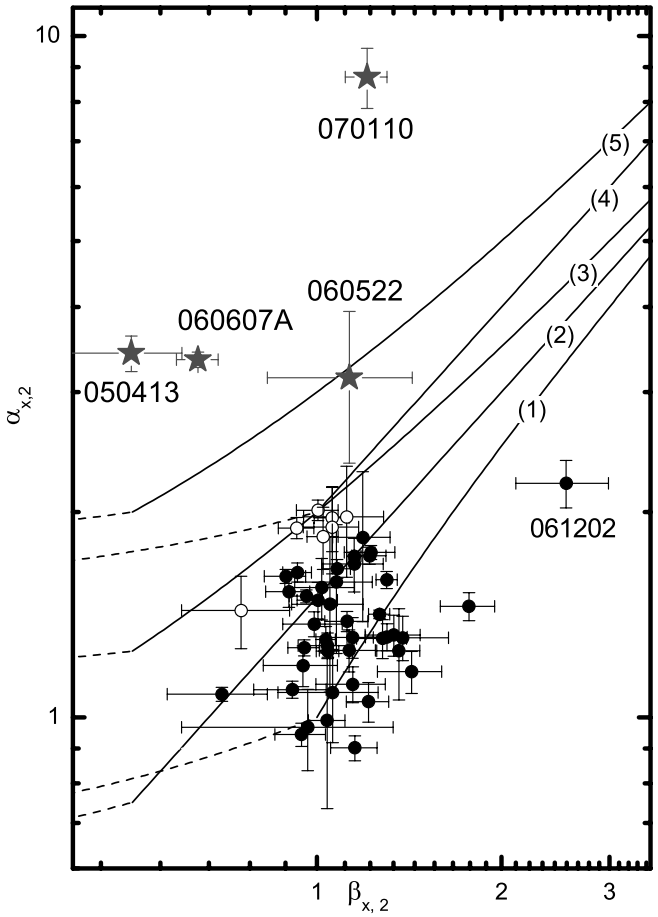

FIG. 6.—Temporal decay index $\alpha_{X,2}$ as a function of the spectral index $\beta_{X,2}$ for the postbreak segment, compared with the closure correlations of various external shock afterglow models: (1) $\nu > \max(\nu_c, \nu_m)$; (2) $\nu_m < \nu < \nu_c$ (ISM, slow cooling); (3) $\nu_m < \nu < \nu_c$ (wind, slow cooling); (4) $\nu > \nu_c$ (jet, slow cooling); (5) $\nu_m < \nu < \nu_c$ (jet, slow cooling). The solid lines are for an electron distribution index $p > 2$, and the dashed lines are for $p < 2$. The filled circles represent the bursts whose $\alpha_{X,2}$ and $\beta_{X,2}$ satisfy models 1 and 2, and the open circles represent those bursts that can be explained with model 3. The stars are those bursts that significantly deviate from the external-shock afterglow models, including GRB 060522 (see discussion in the text). [*See the electronic edition of the Journal for a color version of this figure.*]

is that the plateau is powered by tapping the spin-down energy of the central engine, as suggested by Troja et al. (2007).

5. ENERGY INJECTION BEHAVIOR

As shown above, the normal decay phases for most of the bursts in our sample (49 out of 53) are consistent with the external-shock models. This suggests that, in general, the observed shallow decay phase is also of external origin and may be related to continuous injection of energy into the fireball. In this section, we assume the standard energy injection model and infer from the data the parameters of the long-lived central engine.

We describe the energy injection behavior as $L(t) \propto t^{-q}$ (see, e.g., Zhang & Mészáros 2001).[8] The difference between the decay slopes before and after t_b depends on the observed spectral regime and the type of ambient medium, which can be summarized as

$$\Delta\alpha = \begin{cases} \frac{1}{4}(p+2)(1-q), & \text{regime I, ISM and wind,} \\ \frac{1}{4}(p+3)(1-q), & \text{regime II, ISM,} \\ \frac{1}{4}(p+1)(1-q), & \text{regime II, wind} \end{cases} \quad (5)$$

(derived from Table 2 of Zhang et al. 2006), where p is the power-law index of the electron distribution. The value of p is derived from the observed spectral index, depending on the observed spectral regime. We identify the spectral regime for these bursts by comparing the observed $\alpha_{X,2}$ and $\beta_{X,2}$ with the closure correlations, and we then derive their q-values from equation (5). The distributions of these GRBs in the two-dimensional q-$\Delta\alpha$ and q-p planes are shown in Figure 7, along with the contours of constant p and $\Delta\alpha$ derived from the models (eq. [5]). No correlation between α_1 and α_2 is found. The steepening index $\Delta\alpha$ is found to vary among bursts, with an average of 1.11 ± 0.39. The p-values range from 2 to 3.5 without evidence of clustering (see also Shen et al. 2006). The q-values for most bursts are around -0.75 to 0.55, with an average of about -0.07 ± 0.35. It is worth commenting that a specific energy injection model invoking a spinning-down pulsar predicts a q-value of zero (Dai & Lu 1998a; Zhang & Mészáros 2001). The average q is close to this model prediction.

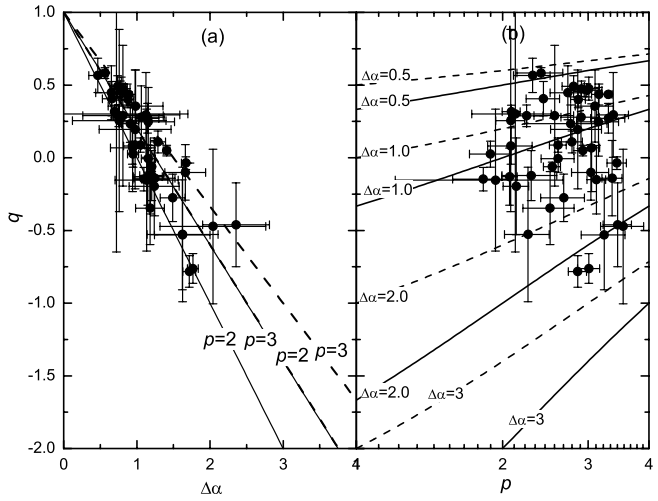

FIG. 7.—Distributions of the 49 GRBs whose normal decay phases are consistent with the external-shock models in the (*a*) q-$\Delta\alpha$ and (*b*) q-p planes, along with the model predictions for $\nu > \max(\nu_c, \nu_m)$ (*solid lines*) and $\nu_m < \nu < \nu_c$ (*dashed lines*).

6. EMPIRICAL RELATION AMONG E_{iso}, E_p, AND t_b

An empirical relation among E_{iso}, E'_p, and $t'_{b,opt}$ was discovered from pre-*Swift* GRBs, where $t'_{b,opt}$ is the temporal break of the optical afterglow light curve in the rest frame of the burst (the Liang-Zhang relation; Liang & Zhang 2005).[9] Willingale et al. (2007) found a correlation similar to the Ghirlanda relation by

[8] Another injection scenario invoking a distribution of the Lorentz factor of the ejecta (Rees & Mészáros 1998) can be effectively represented by a long-term central engine (Zhang et al. 2006). The internal-origin plateaus discussed above suggest that at least for some GRBs, a long-lived central engine is indeed in operation.

[9] If $t'_{b,opt}$ is interpreted as a jet break, then the relation is similar to the Ghirlanda relation (Ghirlanda et al. 2004). However, the more empirical Liang-Zhang relation allows more freedom to understand the origin of the breaks.

assuming that the t_b's in the X-ray band are jet breaks. Such a relation may be interpreted as an effective $E_{\rm iso}$-E'_p-t'_b relation similar to the Liang-Zhang relation. In this section we investigate the relations among the energies $E^b_{\rm iso,\gamma}$ and $E_{\rm iso,X}$ and the other two parameters E'_p and t'_b. With the data reported in Table 4 (for bursts with redshift measurements), we use a multivariate regression analysis to search for possible dependences of $E_{\rm iso,X}$ and $E^b_{\rm iso,\gamma}$ on both E'_p and t'_b. Our sample is limited to those bursts whose t_b can be explained as an energy injection break (without considering the achromatism of the break). Among the 49 bursts, 27 have redshift measurements. Since only two bursts in the internal-origin plateau sample have redshift measurements, we cannot perform an analysis of them. Our regression model reads

$$\log \hat{E}_{\rm iso} = \kappa_0 + \kappa_1 \log E'_p + \kappa_2 \log t'_b, \qquad (6)$$

where $E'_p = E_p(1+z)$ and $t'_b = t_b/(1+z)$. We measure the significance of the dependence of each variable on the model by the probability from a t-test (p_t). The significance of the global regression is measured by an F-test (with a chance probability p_F). Statistically, a robust statistical analysis requires the chance probability to be less than 10^{-4}. Our multiple regression analysis applied to $E_{\rm iso,X}(E'_p, t'_b)$ yields $\kappa_0 = 44.0 \pm 1.1$ (with $p_t < 10^{-4}$), $\kappa_1 = 1.82 \pm 0.33$ (with $p_t < 10^{-4}$), and $\kappa_2 = 0.61 \pm 0.18$ (with $p_t = 3 \times 10^{-3}$). The p_F is less than 10^{-4}. These results suggest a strong correlation between $E_{\rm iso,X}$ and E'_p and a tentative correlation between $E_{\rm iso,X}$ and t'_b. On the other hand, our multiple regression analysis applied to $E^b_{\rm iso,\gamma}(E'_p, t'_b)$ gives $\kappa_0 = 48.3 \pm 0.8$ (with $p_t < 10^{-4}$), $\kappa_1 = 1.70 \pm 0.25$ (with $p_t < 10^{-4}$), and $\kappa_2 = 0.07 \pm 0.13$ (with $p_t = 0.486$). The p_F is less than 10^{-4}. The correlation between $E^b_{\rm iso,\gamma}$ and E'_p is significant, but statistically no correlation between $E^b_{\rm iso,\gamma}$ and t'_b can be claimed.

With the relation discovered by Willingale et al. (2007), one would naively expect a multiple correlation among $E^b_{\rm iso,\gamma}$, E'_p, and t'_b. According to our results, a significant correlation among these variables can indeed be claimed with a chance probability $p_F < 10^{-4}$. However, this correlation is dominated by the correlation of $E^b_{\rm iso,\gamma}$ and E'_p only (with $p_t < 10^{-4}$), which is essentially the Amati relation (Amati et al. 2002). The p_t of the dependence between $E^b_{\rm iso,\gamma}$ and t'_b is 0.486. This strongly rules out such a dependence. Therefore, we suspect that the apparent relation found by Willingale et al. (2007) may intrinsically be a manifestation of the Amati relation. A similar conclusion has also been reached by Nava et al. (2007). The t_b essentially did not enter the problem, since the distribution of t_b is narrower than that of $t_{b,\rm opt}$, as discussed in Liang & Zhang (2005).

It is interesting to note the dependence $E_{\rm iso,X} \propto t'^{\,0.61\pm0.18}_b$. This is in sharp contrast to the Liang-Zhang relation, in which $E_{\rm iso,\gamma} \propto t'^{\,-1.24}_{b,\rm opt}$ was discovered. In order to compare the $E_{\rm iso,X}$-E'_p-t'_b correlation with the Liang-Zhang relation in a two-dimensional plane, we define $\Sigma = \log E_{\rm iso} - \kappa_2 \log t'_b$ and show $\Sigma_{\rm X}$ and Σ_γ as a function of $\log E'_p$ in Figure 8. We observe that the $E_{\rm iso,X}$-E'_p-t'_b correlation is significant, but it has a larger scatter than the Liang-Zhang relation. Although we cannot rule out the possibility that the large dispersion is intrinsic, the observational uncertainties on both $E_{\rm iso,X}$ and E_p could produce such a dispersion. Figure 8 evidently shows that the $E_{\rm iso,X}$-E_p-t_b correlation is different from the Liang-Zhang relation. This suggests that t_b and $t_{b,\rm opt}$ may have distinct physical origins. The positive correlation between $E_{\rm iso,X}$ and t_b is consistent with an energy injection origin for t_b, namely, a longer injection episode giving more energy. The negative correlation between $E_{\rm iso,\gamma}$ and $t_{b,\rm opt}$ may trace back to the standard energy-reservoir argument of Frail et al. (2001), which suggests a connection between $t_{b,\rm opt}$ and the opening angle of the outflow.

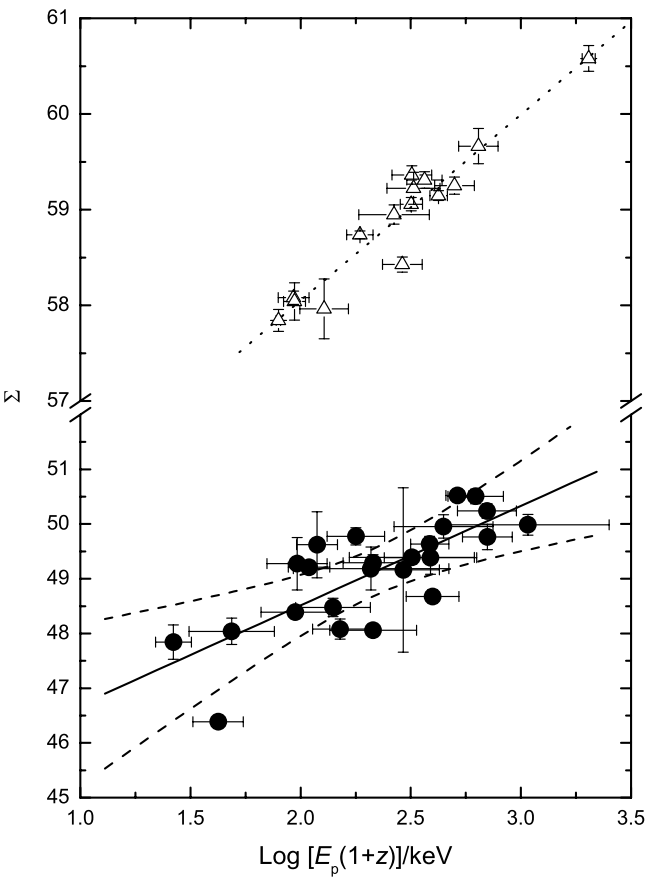

FIG. 8.—Comparison of the $E_{\rm iso,X}$-E'_p-t'_b relation with the bursts in our sample (*filled circles*; the solid and dashed lines mark the best fit and 3 σ level) with the Liang-Zhang relation derived with pre-*Swift* bursts (*open triangles*; the dotted line is the best fit [Liang & Zhang 2005]), where $\Sigma_{\rm X} \equiv \log E_{\rm iso,X} - \kappa_2 t'_b$ and $\Sigma_\gamma \equiv \log E_{\rm iso,\gamma} - \kappa_2 t'_{b,o}$.

7. CONCLUSIONS AND DISCUSSION

We have presented a comprehensive analysis of the *Swift* XRT light curves of long GRBs, focusing on the properties of the shallow decay phase and its relation to the following decay phase. Our sample includes 53 bursts whose X-ray emission was bright enough to allow spectral and temporal analyses for both phases. We summarize our results as follows:

1. We find that the distributions of the characteristic properties of the shallow decay phase are lognormal or normal, that is, $\log t_b({\rm s}) = 4.09 \pm 0.61$, $\log S_{\rm X}({\rm ergs\ cm^{-2}}) = -6.52 \pm 0.69$, $\Gamma_{\rm X,1} = 2.09 \pm 0.21$, and $\alpha_1 = 0.35 \pm 0.35$ (quoted errors are at the 1 σ confidence level).

2. The $E_{\rm iso,X}$ of the shallow decay phase is linearly correlated with the prompt gamma-ray phase, that is, $\log E_{\rm iso,X} = (1.00 \pm 0.16) \log E_{\rm iso,\gamma} - (0.5 \pm 8.10)$ (with a Spearman correlation coefficient $r = 0.79$ and a chance probability $p < 10^{-4}$). The spectrum of the shallow decay phase is softer than that of the prompt gamma-ray phase, except for some typical X-ray flashes.

3. Aside from GRB 061202, no spectral evolution is observed during the transition from the shallow decay to the follow-up decay phase. The postbreak phase in most bursts is consistent with the closure relations of the external-shock models. Six of the 13 bursts with well-sampled optical light curves show an achromatic

break in both X-ray and optical bands, but the other seven cases do not show any break or else have a break at a different epoch in the optical band. This poses the issue of explaining the t_b of these bursts as the end of the energy injection phase.

4. Four bursts in our sample (GRBs 060413, 060522, 060607A, and 070110) have a postbreak phase significantly deviant from the external-shock models. The decay indices are much steeper than model requirements. The optical light curves of the latter two bursts evolve distinctly from the X-ray light curves. We suggest that the X-ray and optical emission of these bursts are from different emission sites and that the X-ray plateaus are of internal origin and demand a long-lived emission component from the central engine.

5. Within the scenario of refreshed external shocks, the average energy injection index $q \sim 0$, suggesting a roughly constant injection luminosity from the central engine.

6. From a subsample of 27 bursts with known redshifts that satisfy the closure relations of the standard external fireball models, we discover an empirical multivariate relation among $E_{\rm iso,X}$, E'_p, and t'_b (eq. [6]), which is distinctly different from the $E_{\rm iso,\gamma}$-E'_p-$t'_{b,\rm opt}$ relation discussed in Liang & Zhang (2005).

7. There is no significant correlation between t'_b and the other parameters $E_{\rm iso,\gamma}$ and E'_p (unlike $t'_{b,\rm opt}$). This suggests that the apparent $E_{j,\gamma}$-E'_p relation found by assuming a jet origin for t_b (Willingale et al. 2007) is likely a manifestation of the Amati relation.

These results suggest that the shallow decay segment observed in most bursts is consistent with an external forward shock origin, probably due to a continuous energy injection into the forward shock from a long-lived central engine. Therefore, scenarios that completely abandon the external-shock models (e.g., Ghisellini et al. 2007; Genet et al. 2007; Uhm & Beloborodov 2007; Shao & Dai 2007) may not be demanded by the data, and these models need to explain the apparent consistency of the α-β data with the simple closure relations of the forward-shock models.

Since the energy injection break is due to a hydrodynamic effect, achromatism is one key feature of the model. Although about half the cases satisfy this constraint, at least some X-ray breaks are chromatic (even if the postbreak segment is well consistent with the standard afterglow model). This poses a great issue to arguing that these are energy injection breaks. Invoking different emission regions (e.g., Zhang & Mészáros 2002) may solve the problem, although more detailed modeling is needed. Crossing of a cooling break would also result in a temporal break, but it would also lead to a change of the spectral index by $\sim$0.5. From Table 1, we find that the changes in the X-ray spectral indices across the breaks of these bursts are 0.01 ± 0.10 (GRB 050318), 0.04 ± 0.10 (GRB 050319), 0.08 ± 0.12 (GRB 050401), and 0.03 ± 0.09 (GRB 050802). These results confidently rule out such a possibility. Genet et al. (2007) account for these chromatic breaks as being due to a long-lived reverse shock in which only a small fraction of the electrons are accelerated. The main issue for such an interpretation is how to "hide" the emission from the forward shock, which carries most of the energy.

Assuming a simple energy injection law $L(t) \propto t^{-q}$, we find that, on average, the injection luminosity could be almost a constant. This places some constraints on physical models for the energy injection scenario. A constant injection luminosity would agree with expectations for energy injection from a central pulsar (Dai & Lu 1998a; Zhang & Mészáros 2001), suggesting that the pulsar injection model may be consistent with the data for at least some GRBs (see also Fan & Xu 2006; De Pasquale et al. 2007; Grupe et al. 2007; Yu et al. 2007).

The temporal decay slopes of some bursts following the shallow decay phase are shallower than the model predictions (Fig. 5; see also Fig. 5 [*top left*] of Willingale et al. 2007). This discrepancy may be alleviated in different ways. First, as shown in Figure 1, α_2 could be systematically steeper if a smoother broken power law model (with smaller ω) were adopted. Second, theoretically the temporal breaks involving external shocks are usually not sharp. Other effects, such as delay of the transfer of the fireball energy to the forward shock (Kobayashi & Zhang 2007) and the structured-jet effect (Kumar & Granot 2003; Zhang et al. 2004; Yamazaki et al. 2006) would modify the simplest closure relations to create a band rather than a line in the α-β plane.

One interesting conclusion from this study is that for at least a small fraction of bursts (e.g., GRBs 060413, 060522, 060607A, and 070110), the observed shallow decay phase is likely of internal origin. This is another component other than X-ray flares that is possibly of internal origin. Unlike the erratic X-ray flares, this component has a smoother light curve with flickering, likely due to a steady component from the central engine. A possible energy source for such a component is the spin energy from the central engine, and an internal dissipation of the spin-down power may be the origin (e.g., Troja et al. 2007). Tapping of the rotational energy would likely be through magnetic fields, either through dipolar spin-down for a central millisecond pulsar (Usov 1992; Dai & Lu 1998a, 1998b; Zhang & Mészáros 2001) or by the Blandford-Znajek mechanism for a black hole central engine (Blandford & Znajek 1977; Mészáros & Rees 1997b; Li 2000). If one accepts that such a component is common among bursts, one can speculate that the observed early X-ray emission is the sum of different emission components. The competition among these components shapes the variety of X-ray light curves that one observes. Depending on the relative importance of the internal and external components, the shallow decay segment could possibly be dominated by either the radiation from the refreshed shocks or by the steady radiation component from the internal dissipation of the central engine. In the former scenario, the shallow decay phase undergoes a transition to a normal decay phase that is consistent with the external-shock models. In the latter scenario, the emission level of the underlying afterglow component is weaker than that from the emission component of the central engine, so that one needs a steep dropoff from the plateau to land on the external-shock emission component.

We acknowledge the use of the public data from the *Swift* archive. We appreciate valuable comments and suggestions from the anonymous referee and from P. O'Brien, Z.-G. Dai, X. Dai, D.-M. Wei, K. Ioka, L. Nava, X.-Y. Wang, X.-F. Wu, and F.-W. Zhang. This work was supported by NASA under grants NNG06GH62G, NNG05GB67G, NNX07AJ64G, and NNX07AJ66G and by the National Natural Science Foundation of China under grants 10463001 (E.-W. L.) and 10640420144.

REFERENCES

Amati, L., et al. 2002, A&A, 390, 81
Asfandyarov, I., Pozanenko, A., & Ibrahimov, M. 2006, GCN Circ. 5434, http://gcn.gsfc.nasa.gov/gcn/gcn3/5434.gcn3
Barbier, L., Barthelmy, S., Cummings, J., Krimm, H., Markwardt, C., Palmer, D., Sakamoto, T., & Tueller, J. 2006a, GCN Circ. 5091, http://gcn.gsfc.nasa.gov/gcn/gcn3/5091.gcn3
Barbier, L., et al. 2005, GCN Circ. 4104, http://gcn.gsfc.nasa.gov/gcn/gcn3/4104.gcn3
———. 2006b, GCN Circ. 4961, http://gcn.gsfc.nasa.gov/gcn/gcn3/4961.gcn3
———. 2006c, GCN Circ. 5108, http://gcn.gsfc.nasa.gov/gcn/gcn3/5108.gcn3
———. 2006d, GCN Circ. 5403, http://gcn.gsfc.nasa.gov/gcn/gcn3/5403.gcn3
Barthelmy, S., et al. 2005a, GCN Circ. 3682, http://gcn.gsfc.nasa.gov/gcn/gcn3/3682.gcn3

Barthelmy, S., et al. 2005b, GCN Circ. 4077, http://gcn.gsfc.nasa.gov/gcn/gcn3/4077.gcn3
———. 2006a, GCN Circ. 5256, http://gcn.gsfc.nasa.gov/gcn/gcn3/5256.gcn3
———. 2006b, GCN Circ. 5421, http://gcn.gsfc.nasa.gov/gcn/gcn3/5421.gcn3
Berger, E., Cenko, S. B., Steidel, C., Reddy, N., & Fox, D. B. 2005, GCN Circ. 3368, http://gcn.gsfc.nasa.gov/gcn/gcn3/3368.gcn3
Berger, E., & Gladders, M. 2006, GCN Circ. 5170, http://gcn.gsfc.nasa.gov/gcn/gcn3/5170.gcn3
Berger, E., & Mulchaey, J. 2005, GCN Circ. 3122, http://gcn.gsfc.nasa.gov/gcn/gcn3/3122.gcn3
Blandford, R. D., & Znajek, R. L. 1977, MNRAS, 179, 433
Bloom, J. S., Frail, D. A., & Sari, R. 2001, AJ, 121, 2879
Bloom, J. S., Perley, D. A., & Chen, H.-W. 2006, GCN Circ. 5826, http://gcn.gsfc.nasa.gov/gcn/gcn3/5826.gcn3
Bloom, J. S., Perley, D., Foley, R., Prochaska, J. X., Chen, H.-W., & Starr, D. 2005, GCN Circ. 3758, http://gcn.gsfc.nasa.gov/gcn/gcn3/3758.gcn3
Burrows, D. N., et al. 2004, Proc. SPIE, 5165, 201
———. 2005, Science, 309, 1833
Butler, N. R., & Kocevski, D. 2007, ApJ, 668, 400
Cabrera, J. I., Firmani, C., Avila-Reese, V., Ghirlanda, G., Ghisellini, G., & Nava, L. 2007, MNRAS, in press (arXiv:0704.0791)
Campana, S., et al. 2006, Nature, 442, 1008
Castro-Tirado, A. J., Amado, P., Negueruela, I., Gorosabel, J., Jelínek, M., & de Ugarte Postigo, A. 2006, GCN Circ. 5218, http://gcn.gsfc.nasa.gov/gcn/gcn3/5218.gcn3
Cenko, S. B., Berger, E., & Cohen, J. 2006a, GCN Circ. 4592, http://gcn.gsfc.nasa.gov/gcn/gcn3/4592.gcn3
Cenko, S. B., Berger, E., Djorgovski, S. G., Mahabal, A. A., & Fox, D. B. 2006b, GCN Circ. 5155, http://gcn.gsfc.nasa.gov/gcn/gcn3/5155.gcn3
Cenko, S. B., Kulkarni, S. R., Gal-Yam, A., & Berger, E. 2005, GCN Circ. 3542, http://gcn.gsfc.nasa.gov/gcn/gcn3/3542.gcn3
Chevalier, R. A., & Li, Z.-Y. 2000, ApJ, 536, 195
Cucchiara, A., Fox, D. B., & Berger, E. 2006a, GCN Circ. 4729, http://gcn.gsfc.nasa.gov/gcn/gcn3/4729.gcn3
Cucchiara, A., Price, P. A., Fox, D. B., Cenko, S. B., & Schmidt, B. P. 2006b, GCN Circ. 5052, http://gcn.gsfc.nasa.gov/gcn/gcn3/5052.gcn3
Cummings, J., et al. 2005, GCN Circ. 2992, http://gcn.gsfc.nasa.gov/gcn/gcn3/2992.gcn3
———. 2006, GCN Circ. 5443, http://gcn.gsfc.nasa.gov/gcn/gcn3/5443.gcn3
———. 2007, GCN Circ. 6007, http://gcn.gsfc.nasa.gov/gcn/gcn3/6007.gcn3
Curran, P. A., et al. 2007, A&A, 467, 1049
Dai, X., Halpern, J. P., Morgan, N. D., Armstrong, E., Mirabal, N., Haislip, J. B., Reichart, D. E., & Stanek, K. Z. 2007, ApJ, 658, 509
Dai, Z.-G. 2004, ApJ, 606, 1000
Dai, Z.-G., & Cheng, K. S. 2001, ApJ, 558, L109
Dai, Z.-G., & Lu, T. 1998a, A&A, 333, L87
———. 1998b, Phys. Rev. Lett., 81, 4301
Dai, Z.-G., Wang, X.-Y., Wu, X.-F., & Zhang, B. 2006, Science, 311, 1127
Della Valle, M., et al. 2006, Nature, 444, 1050
De Pasquale, M., et al. 2006, MNRAS, 365, 1031
———. 2007, MNRAS, 377, 1638
Dermer, C. D. 2007, ApJ, 664, 384
Eichler, D., & Granot, J. 2006, ApJ, 641, L5
Fan, Y., & Piran, T. 2006, MNRAS, 369, 197
Fan, Y.-Z., & Wei, D.-M. 2005, MNRAS, 364, L42
Fan, Y.-Z., & Xu, D. 2006, MNRAS, 372, L19
Fenimore, E., et al. 2005, GCN Circ. 4217, http://gcn.gsfc.nasa.gov/gcn/gcn3/4217.gcn3
———. 2006a, GCN Circ. 5295, http://gcn.gsfc.nasa.gov/gcn/gcn3/5295.gcn3
———. 2006b, GCN Circ. 5831, http://gcn.gsfc.nasa.gov/gcn/gcn3/5831.gcn3
Frail, D. A., et al. 2001, ApJ, 562, L55
Fynbo, J. P. U., Hjorth, J., Jensen, B. L., Jakobsson, P., Møller, P., & Näränen, J. 2005a, GCN Circ. 3136, http://gcn.gsfc.nasa.gov/gcn/gcn3/3136.gcn3
Fynbo, J. P. U., et al. 2005b, GCN Circ. 3176, http://gcn.gsfc.nasa.gov/gcn/gcn3/3176.gcn3
———. 2005c, GCN Circ. 3749, http://gcn.gsfc.nasa.gov/gcn/gcn3/3749.gcn3
———. 2006, Nature, 444, 1047
Gal-Yam, A., et al. 2006, Nature, 444, 1053
Gehrels, N., et al. 2004, ApJ, 611, 1005 (erratum 621, 558)
———. 2006, Nature, 444, 1044
Genet, F., Daigne, F., & Mochkovitch, R. 2007, MNRAS, submitted (astro-ph/0701204)
Ghirlanda, G., Ghisellini, G., & Lazzati, D. 2004, ApJ, 616, 331
Ghisellini, G., Ghirlanda, G., Nava, L., & Firmani, C. 2007, ApJ, 658, L75
Golenetskii, S., Aptekar, R., Mazets, E., Pal'shin, V., Frederiks, D., & Cline, T. 2006, GCN Circ. 5446, http://gcn.gsfc.nasa.gov/gcn/gcn3/5446.gcn3
Gou, L.-J., Dai, Z.-G., Huang, Y.-F., & Lu, T. 2001, A&A, 368, 464
Granot, J., Königl, A., & Piran, T. 2006, MNRAS, 370, 1946
Granot, J., & Kumar, P. 2006, MNRAS, 366, L13
Grupe, D., et al. 2007, ApJ, 662, 443
Huang, K.-Y., et al. 2007, ApJ, 654, L25
Hullinger, D., et al. 2005a, GCN Circ. 3364, http://gcn.gsfc.nasa.gov/gcn/gcn3/3364.gcn3
———. 2005b, GCN Circ. 3856, http://gcn.gsfc.nasa.gov/gcn/gcn3/3856.gcn3
———. 2006, GCN Circ. 4851, http://gcn.gsfc.nasa.gov/gcn/gcn3/4851.gcn3
Ioka, K., Toma, K., Yamazaki, R., & Nakamura, T. 2006, A&A, 458, 7
Jakobsson, P., Levan, A., Chapman, R., Rol, E., Tanvir, N., Vreeswijk, P., & Watson, D. 2006a, GCN Circ. 5617, http://gcn.gsfc.nasa.gov/gcn/gcn3/5617.gcn3
Jakobsson, P., Tanvir, N., Jensen, B. L., Fynbo, J. P. U., de Ugarte Postigo, A., Gorosabel, J., Klose, S., & Vreeswijk, P. 2006b, GCN Circ. 5298, http://gcn.gsfc.nasa.gov/gcn/gcn3/5298.gcn3
Jakobsson, P., et al. 2006c, A&A, 460, L13
Jaunsen, A. O., Malesani, D., Fynbo, J. P. U., Sollerman, J., & Vreeswijk, P. M. 2007, GCN Circ. 6010, http://gcn.gsfc.nasa.gov/gcn/gcn3/6010.gcn3
Jin, Z.-P., Yan, T., Fan, Y.-Z., & Wei, D.-M. 2007, ApJ, 656, L57
Kelson, D., & Berger, E. 2005, GCN Circ. 3101, http://gcn.gsfc.nasa.gov/gcn/gcn3/3101.gcn3
King, A., O'Brien, P. T., Goad, M. R., Osborne, J., Olsson, E., & Page, K. 2005, ApJ, 630, L113
King, I. R. 1971, PASP, 83, 199
Kobayashi, S., & Zhang, B. 2007, ApJ, 655, 973
Krimm, H., et al. 2005a, GCN Circ. 3105, http://gcn.gsfc.nasa.gov/gcn/gcn3/3105.gcn3
———. 2005b, GCN Circ. 3119, http://gcn.gsfc.nasa.gov/gcn/gcn3/3119.gcn3
———. 2005c, GCN Circ. 3134, http://gcn.gsfc.nasa.gov/gcn/gcn3/3134.gcn3
———. 2006a, GCN Circ. 5153, http://gcn.gsfc.nasa.gov/gcn/gcn3/5153.gcn3
———. 2006b, GCN Circ. 5334, http://gcn.gsfc.nasa.gov/gcn/gcn3/5334.gcn3
———. 2006c, GCN Circ. 6058, http://gcn.gsfc.nasa.gov/gcn/gcn3/6058.gcn3
Kumar, P., & Granot, J. 2003, ApJ, 591, 1075
Kumar, P., & Panaitescu, A. 2000a, ApJ, 541, L9
———. 2000b, ApJ, 541, L51
Lamb, D., et al. 2006, GCN Circ. 4601, http://gcn.gsfc.nasa.gov/gcn/gcn3/4601.gcn3
Lazzati, D., & Begelman, M. C. 2006, ApJ, 641, 972
Ledoux, C., Vreeswijk, P., Smette, A., Jaunsen, A., & Kaufer, A. 2006, GCN Circ. 5237, http://gcn.gsfc.nasa.gov/gcn/gcn3/5237.gcn3
Li, L.-X. 2000, ApJ, 540, L17
Liang, E., & Zhang, B. 2005, ApJ, 633, 611
Liang, E.-W., Racusin, J. L., Zhang, B., Zhang, B.-B., & Burrows, D. N. 2007, ApJ, submitted (arXiv:0708.2942)
Liang, E.-W., et al. 2006, ApJ, 646, 351
Mangano, V., et al. 2007, A&A, 470, 105
Markwardt, C., et al. 2006a, GCN Circ. 4435, http://gcn.gsfc.nasa.gov/gcn/gcn3/4435.gcn3
———. 2006b, GCN Circ. 4671, http://gcn.gsfc.nasa.gov/gcn/gcn3/4671.gcn3
———. 2006c, GCN Circ. 5022, http://gcn.gsfc.nasa.gov/gcn/gcn3/5022.gcn3
———. 2006d, GCN Circ. 5174, http://gcn.gsfc.nasa.gov/gcn/gcn3/5174.gcn3
Mason, K. O., et al. 2006, ApJ, 639, 311
McGowan, K., Band, D., Brown, P., Gronwall, C., Huckle, H., & Hancock, B. 2005a, GCN Circ. 3739, http://gcn.gsfc.nasa.gov/gcn/gcn3/3739.gcn3
McGowan, K., Morgan, A., Mason, K., & Kennedy, T. 2005b, GCN Circ. 3745, http://gcn.gsfc.nasa.gov/gcn/gcn3/3745.gcn3
Melandri, A., Grazian, A., Guidorzi, C., Monfardini, A., Mundell, C. G., & Gomboc, A. 2006, GCN Circ. 4539, http://gcn.gsfc.nasa.gov/gcn/gcn3/4539.gcn3
Mészáros, P. 2002, ARA&A, 40, 137
———. 2006, Rep. Prog. Phys., 69, 2259
Mészáros, P., & Rees, M. J. 1997a, ApJ, 476, 232
———. 1997b, ApJ, 482, L29
Misra, K., Bhattacharya, D., Sahu, D. K., Sagar, R., Anupama, G. C., Castro-Tirado, A. J., Guziy, S. S., & Bhatt, B. C. 2007, A&A, 464, 903
Molinari, E., et al. 2007, A&A, 469, L13
Nava, L., Ghisellini, G., Ghirlanda, G., Cabrera, J. I., Firmani, C., & Avila-Reese, V. 2007, MNRAS, 377, 1464
Nousek, J. A., et al. 2006, ApJ, 642, 389
O'Brien, P. T., Willingale, R., Osborne, J. P., & Goad, M. R. 2006a, New J. Phys., 8, 121
O'Brien, P. T., et al. 2006b, ApJ, 647, 1213
Page, K. L., et al. 2007, ApJ, 663, 1125
Palmer, D., et al. 2005, GCN Circ. 3737, http://gcn.gsfc.nasa.gov/gcn/gcn3/3737.gcn3
———. 2006a, GCN Circ. 4476, http://gcn.gsfc.nasa.gov/gcn/gcn3/4476.gcn3
———. 2006b, GCN Circ. 5744, http://gcn.gsfc.nasa.gov/gcn/gcn3/5744.gcn3
———. 2006c, GCN Circ. 5551, http://gcn.gsfc.nasa.gov/gcn/gcn3/5551.gcn3
Panaitescu, A. 2007, MNRAS, 379, 331

Panaitescu, A., Mészáros, P., Burrows, D., Nousek, J., Gehrels, N., O'Brien, P., & Willingale, R. 2006a, MNRAS, 369, 2059
Panaitescu, A., Mészáros, P., Gehrels, N., Burrows, D., & Nousek, J. 2006b, MNRAS, 366, 1357
Panaitescu, A., Mészáros, P., & Rees, M. J. 1998, ApJ, 503, 314
Parsons, A., et al. 2005a, GCN Circ. 3600, http://gcn.gsfc.nasa.gov/gcn/gcn3/3600.gcn3
———. 2005b, GCN Circ. 3757, http://gcn.gsfc.nasa.gov/gcn/gcn3/3757.gcn3
———. 2006a, GCN Circ. 4912, http://gcn.gsfc.nasa.gov/gcn/gcn3/4912.gcn3
———. 2006b, GCN Circ. 5053, http://gcn.gsfc.nasa.gov/gcn/gcn3/5053.gcn3
———. 2006c, GCN Circ. 5214, http://gcn.gsfc.nasa.gov/gcn/gcn3/5214.gcn3
———. 2006d, GCN Circ. 5370, http://gcn.gsfc.nasa.gov/gcn/gcn3/5370.gcn3
———. 2006e, GCN Circ. 5561, http://gcn.gsfc.nasa.gov/gcn/gcn3/5561.gcn3
Pavlenko, E., Efimov, Yu., Shlyapnikov, A., Baklanov, A., Pozanenko, A., & Ibrahimov, M. 2005, GCN Circ. 3744, http://gcn.gsfc.nasa.gov/gcn/gcn3/3744.gcn3
Pavlenko, E., Vasyliskov, K., Palaguta, M., Dulich, Yu., & Pozananko, A. 2006a, GCN Circ. 5324, http://gcn.gsfc.nasa.gov/gcn/gcn3/5324.gcn3
Pavlenko, E., Vasyliskov, K., Palaguta, M., Dulich, Yu., Pozanenko, A., Salyamov, R., & Ibrahimov, M. 2006b, GCN Circ. 5317, http://gcn.gsfc.nasa.gov/gcn/gcn3/5317.gcn3
Pe'er, A., Mészáros, P., & Rees, M. J. 2006, ApJ, 652, 482
Perna, R., Armitage, P. J., & Zhang, B. 2006, ApJ, 636, L29
Piran, T. 2005, Rev. Mod. Phys., 76, 1143
Preece, R. D., Briggs, M. S., Mallozzi, R. S., Pendleton, G. N., Paciesas, W. S., & Band, D. L. 2000, ApJS, 126, 19
Price, P. A., Berger, E., & Fox, D. B. 2006, GCN Circ. 5275, http://gcn.gsfc.nasa.gov/gcn/gcn3/5275.gcn3
Proga, D., & Zhang, B. 2006, MNRAS, 370, L61
Quimby, R., Fox, D., Höflich, P., Roman, B., & Wheeler, J. C. 2005, GCN Circ. 4221, http://gcn.gsfc.nasa.gov/gcn/gcn3/4221.gcn3
Quimby, R. M., et al. 2006, ApJ, 640, 402
Rees, M. J., & Mészáros, P. 1994, ApJ, 430, L93
———. 1998, ApJ, 496, L1
Rhoads, J. E. 1997, ApJ, 487, L1
Rol, E., Jakobsson, P., Tanvir, N., & Levan, A. 2006, GCN Circ. 5555, http://gcn.gsfc.nasa.gov/gcn/gcn3/5555.gcn3
Romano, P., et al. 2006, A&A, 456, 917
Rumyantsev, V., Pavlenko, E., & Pozanenko, A. 2006, GCN Circ. 5336, http://gcn.gsfc.nasa.gov/gcn/gcn3/5336.gcn3
Rykoff, E. S., et al. 2005, ApJ, 631, L121
———. 2006, ApJ, 638, L5
Sakamoto, T., et al. 2005a, GCN Circ. 3173, http://gcn.gsfc.nasa.gov/gcn/gcn3/3173.gcn3
———. 2005c, GCN Circ. 3273, http://gcn.gsfc.nasa.gov/gcn/gcn3/3273.gcn3
———. 2005b, GCN Circ. 3730, http://gcn.gsfc.nasa.gov/gcn/gcn3/3730.gcn3
———. 2006a, GCN Circ. 4445, http://gcn.gsfc.nasa.gov/gcn/gcn3/4445.gcn3
———. 2006b, GCN Circ. 4748, http://gcn.gsfc.nasa.gov/gcn/gcn3/4748.gcn3
———. 2006c, GCN Circ. 5349, http://gcn.gsfc.nasa.gov/gcn/gcn3/5349.gcn3
———. 2006d, GCN Circ. 5887, http://gcn.gsfc.nasa.gov/gcn/gcn3/5887.gcn3
Sakamoto, T., et al. 2007, ApJS, in press (arXiv:0707.4626)
Sari, R., & Mészáros, P. 2000, ApJ, 535, L33
Sari, R., Piran, T., & Halpern, J. P. 1999, ApJ, 519, L17
Sari, R., Piran, T., & Narayan, R. 1998, ApJ, 497, L17
Sato, G., et al. 2006, GCN Circ. 5538, http://gcn.gsfc.nasa.gov/gcn/gcn3/5538.gcn3
Shao, L., & Dai, Z.-G. 2007, ApJ, 660, 1319
Shen, R., Kumar, P., & Robinson, E. L. 2006, MNRAS, 371, 1441
Soderberg, A. M., Berger, E., & Ofek, E. 2005, GCN Circ. 4186, http://gcn.gsfc.nasa.gov/gcn/gcn3/4186.gcn3
Stamatikos, M., et al. 2006a, GCN Circ. 5289, http://gcn.gsfc.nasa.gov/gcn/gcn3/5289.gcn3
———. 2006b, GCN Circ. 5459, http://gcn.gsfc.nasa.gov/gcn/gcn3/5459.gcn3
Stanek, K. Z., et al. 2007, ApJ, 654, L21
Still, M., et al. 2005, ApJ, 635, 1187
Tagliaferri, G., et al. 2005, Nature, 436, 985
Thöne, C. C., et al. 2006, GCN Circ. 5373, http://gcn.gsfc.nasa.gov/gcn/gcn3/5373.gcn3
Toma, K., Ioka, K., Yamazaki, R., & Nakamura, T. 2006, ApJ, 640, L139
Troja, E., et al. 2007, ApJ, 665, 599
Tueller, J., et al. 2006a, GCN Circ. 5242, http://gcn.gsfc.nasa.gov/gcn/gcn3/5242.gcn3
———. 2006b, GCN Circ. 5395, http://gcn.gsfc.nasa.gov/gcn/gcn3/5395.gcn3
———. 2006c, GCN Circ. 5964, http://gcn.gsfc.nasa.gov/gcn/gcn3/5964.gcn3
Uhm, Z. L., & Beloborodov, A. M. 2007, ApJ, 665, L93
Usov, V. V. 1992, Nature, 357, 472
Vaughan, S., et al. 2006, ApJ, 638, 920
Vreeswijk, P., Jakobsson, P., Ledoux, C., Thöne, C., & Fynbo, J. 2006, GCN Circ. 5535, http://gcn.gsfc.nasa.gov/gcn/gcn3/5535.gcn3
Wang, W., & Dai, Z.-G. 2001, Chinese Phys. Lett., 18, 1153
Watson, D., et al. 2006, ApJ, 652, 1011
Wei, D.-M., & Lu, T. 2000, ApJ, 541, 203
Willingale, R., et al. 2007, ApJ, 662, 1093
Yamazaki, R., Toma, K., Ioka, K., & Nakamura, T. 2006, MNRAS, 369, 311
Yost, S. A., et al. 2007, ApJ, 657, 925
Yu, Y.-W., & Dai, Z.-G. 2007, A&A, 470, 119
Yu, Y.-W., Liu, X.-W., & Dai, Z.-G. 2007, ApJ, in press (arXiv:0706.3741)
Zhang, B. 2006, Nature, 444, 1010
———. 2007, Chinese J. Astron. Astrophys., 7, 1 (erratum 7, 329)
Zhang, B., Dai, X., Lloyd-Ronning, N. M., & Mészáros, P. 2004, ApJ, 601, L119
Zhang, B., Fan, Y.-Z., Dyks, J., Kobayashi, S., Mészáros, P., Burrows, D. N., Nousek, J. A., & Gehrels, N. 2006, ApJ, 642, 354
Zhang, B., & Mészáros, P. 2001, ApJ, 552, L35
———. 2002, ApJ, 566, 712
———. 2004, Int. J. Mod. Phys. A, 19, 2385
Zhang, B., Zhang, B.-B., Liang, E.-W., Gehrels, N., Burrows, D. N., & Mészáros, P. 2007a, ApJ, 655, L25
Zhang, B., et al. 2007b, ApJ, 655, 989
Zhang, B.-B., Liang, E.-W., & Zhang, B. 2007c, ApJ, 666, 1002 (Paper I)